A STUDY OF DIVERGING CONCERTINA TEARING OF DUCTILE METAL PLATES

by

KATHERINE A. TRAUTH

S.B. Massachusetts Institute of Technology (1993)

Submitted to the

DEPARTMENT OF OCEAN ENGINEERING

In Partial Fulfillment of the Requirements

For the Degree of

MASTER OF SCIENCE IN OCEAN ENGINEERING

at the

MASSACHUSETTS INSTITUTE OF TECHNOLOGY

SEPTEMBER, 1994

Signature of Author:_____

Department of Ocean Engineering

May, 1994

Certified By:_____

Professor Tomasz Wierzbicki

Thesis Supervisor

Accepted By:_____

Professor A. Douglas Carmichael, Chairman

Departmental Graduate Committee

Department of Ocean Engineering

Abstract

The objective of this paper is the study of failure modes of infinite plates subjected to a piercing loading. This project was conducted as a part of the Joint MIT-Industry Consortium on Tanker Safety. The study has found a mathematical model for diverging concertina tearing with good experimental correlation. The experiments also showed that the concertina and pure cutting failure modes occur at similar force levels, and in a non-ideal situation, i.e. with introduced eccentricities, pre-cuts, and other structural imperfections, a shift between the modes and then back was observed.

Tests were conducted in MIT's Civil Engineering REMERGENCE facilities using an Instron 20 kip Universal Testing Machine. The specimen had three sides bolted into a frame which was attached to the crosshead of the UTM, leaving the top side free for contact with the wedge. In the first series of experiments, the wedge began cutting from a notch cut in the free edge, but the first 10 cm of deformation was governed by the free edge boundary conditions. The next tests were conducted by manufacturing a precut hole below this transition area. The area of the deformation was small compared to the surface area of the sample and thus was not affected by the clamped boundary conditions, therefore modeling an infinite plate.

The samples had an exposed surface area of 290 mm by 560 mm and thickness of 0.4 mm. Most of the tests were run with a crosshead speed of 1 inch per minute, while the wedge was stationary and perpendicular to the direction of travel of the sample. The wedges were of various shapes: blunt, rounded, and 45^{o} rounded; the thicknesses of the wedges were 0.5 in and 0.75 in. The narrow rounded wedge initiated failure in concertina tearing mode, transitioned into cutting, and then returned back into concertina failure. The other wedges each caused a concertina failure mode.

The measured force levels for both the diverging concertina tests and the tests with both concertina and central cutting showed good correlation with the predicted mean force levels. Theory that predicts the folding wavelength and the diverging shape both also show good correlation with the measured data. In addition, formulas were derived for the shape of the diverging tear using a simple fracture criteria. An excellent correlation was obtained with the measured shape of the torn plates.

Acknowledgments

I would like to thank my parents for the love and support that they have given me over my past five years at MIT, and especially for their support in the last two months. I wouldn't have finished this thesis without them.

I would also like to thank Professor Tomasz Wierzbicki for the encouragement, moral and theoretical support he has given me over the past year. Without Arthur and Steve Rudolph in the Civil Engineering Machine shop, none of my experiments could have been conducted. Their exacting work on rush orders and their advice on the Instron were invaluable.

And last, but certainly by far not least in terms of last-minute moral support, commiseration and all around experimental help are the other members of the Joint MIT-Industry Program on Tanker Safety experimental team. They are Mohammed Yahiaoui, Mark Bracco, Pat Little, and Neil Best.

Table of Contents

List of Figures

List of Symbols

ASTM American Standard Testing Materials

b concertina support separation variable

$\dot{E}_b$ rate of bending energy

$\dot{E}_m$ rate of membrane energy

$\dot{E}_s$ rate of shear energy

$\dot{E}_f$ rate of tearing fracture energy

F_m mean force during concertina tearing

H concertina fold length

R specific work of fracture

t plate thickness

$\dot{u}$ wedge velocity

x length of cut in concertina tearing

y_o half initial concertina tear width

$\overline{x} = \frac{x}{t}$ dimensionless cut length

$\overline{y} = \frac{y}{t}$ dimensionless half tear width

$\overline{y}_o = \frac{y_o}{t}$ dimensionless initial half tear width

δ_t crack opening displacement parameter (COD)

θ wedge semi-angle

μ coefficient of friction

σ_o material flow stress

σ_y material yield strength

σ_{ult} ultimate stress

1 Introduction

In the tearing of infinite plates, there are two primary modes of failure. The more common is a central cutting mode, in which the plate is cut longitudinally in front of the wedge, and the displaced metal curls into cylindrical surfaces. The other mode of failure is concertina a tearing. This occurs when the plate "bunches up" before the wedge and the force becomes distributed and causes tearing in two locations roughly equidistant from the longitudinal axis of the wedge. In a longitudinally stiffened plate, the concertina folding extends over the width of the constrained region, tearing along the stiffeners. In an infinite plate, tearing begins at both sides of the edges of the wedge and diverges. The section of the plate ahead of the wedge folds in a fan-fold or "concertina" folding mode. Figure 1.1 shows diverging and constrained concertina shapes.

This paper concentrates on diverging concertina tearing of an infinite plate, but also correlates previously derived theories for constrained concertina tearing. Concertina tearing has been observed both in previous experiments and in actual ship grounding accidents. A section of the hull of an oil tanker involved in a grounding showed a case of concertina tearing, as did experiments performed by Kitamura, et al [1]. This demonstrates that concertina deformation is a mode of failure which occurs in practice and is important in the consideration of ship hull structure.

1.1 Environmental Significance

Over the past fifteen or twenty years, there have been numerous grounding accidents of VLCCs (Very Large Crude Carriers), the EXXON VALDEZ, the American Trader, etc., which have done immeasurable damage to the fragile environment of the Earth's oceans. The most recent accidents have increased the public awareness of the

danger of oil tanker spills. As a consequence of this, the United States government has enacted new, tougher laws concerning the design and manufacture of VLCC hulls, however no in-depth experimental studies were conducted in these areas. The question of double vs. single hull design has been considered. The Joint MIT-Industry Consortium on Oil Tanker Safety arose to address these issues.

In 1990, the U.S. Congress passed the Oil Pollution Act (OPA90). This requires that all U.S. and foreign flag vessels operating in U.S. waters which are constructed after or are overhauled after June 30, 2015 must have a double hull, [2], [3]. Immediately following that, the U.S. Coast Guard began working on a set of acceptable regulations for shipbuilders to follow in order to be in compliance with the Act; now the Coast Guard is also researching studying other designs which might fulfill the spirit, if not the letter of OPA90.

1.2 Prior Research on Wedge Penetration

1.2.1 Central Separation

In research performed in 1993, Leonard Maxwell [4] studied the initiation of central separation and concertina tearing. He found that the central separation tests showed "distinct trends in plate geometry results and force vs. length of cut curves." It was shown that there was good correlation between the proposed theory for the cutting equations for the specified geometry. The cylindrical wedge caused central tearing to occur with a pre-cut for initiation.

In other research which has been conducted on central separation, central cutting occurred with good correlation with theory, however the tests were limited in scope and

only pertained to specific rock and ship geometries, or only under special circumstances. Maxwell attempted to find a correlation between different rock geometries and the initiation of failure. However, he found not only central separation, but also concertina tearing occurred, depending on pre-cut placing and wedge geometry.

Further tests were conducted by the experimental team of the Joint MIT-Industry Consortium on Tanker Safety to support new steady state central cutting theory developed by Zheng and Wierzbicki. At a frame angle of 10^{o}, a thin sheet of steel was started in central cutting from a pre-cut hole using a 45^{o} sharp, 0.75 inch wedge. This caused a central cutting pattern to occur, in which the flaps of steel were pushed away from the cut by the wedge to the "downward" side of the sample. The initiation occurred as Maxwell had predicted, and then the cutting quickly became steady state.

1.2.2 Braided Cut

Earlier attempts at steady-state central cutting caused a braided pattern to occur, similar to the edge of a lasagna noodle. Using a 0.5 inch 45^{o} sharp wedge, central cutting was obtained on thin, 0.4 mm steel plate. However, with no tilt angle, the flaps did not have a "downward" side to be pushed to. This caused the flaps to fold alternating to each side of the sample. In much the same manner of alternating folds as is found in concertina tearing, the metal cut ahead of the wedge until a point, and then began to fold. However, due to its geometry, the wedge would then cut through the folded metal causing the flaps to alternate to the other side of the sample. Theory for this failure mode has not yet been developed, but it was observed that the average force level for the braided steady state central cutting was very similar to the force level of the standard steady state central cutting.

Both the braided and standard central separation were observed in the experiments which alternated between the cutting and concertina tearing modes. As will be discussed later, the average force levels for not only the two types of central separation, but also the forces for diverging concertina are similar.

1.2.3 Bounded Concertina Tearing

In the tests conducted by Maxwell, concertina tearing occurred across the entire width of the sample. The frame of the apparatus simulated longitudinal stiffeners for the plate, and the sample was torn at the boundary of the plate. Again, Maxwell was not able to achieve steady-state deformation because of the shortness of the stroke of the testing machine; however, enough concertina folds were formed that the failure would continue in a concertina tearing mode.

When double hull tests were begun by the Joint Consortium on Tanker Safety experimental team, it was found that concertina folding occurred between the stiffeners in the specimen. The tearing diverged until it reached the stiffeners, and then continued the length of the plate bounded by the stiffeners. An additional test was run with a single hull, longitudinally stiffened plate. Using a wedge with a width equal to half the distance between the stiffeners and precuts at the stiffeners, bounded concertina occurred. This experiment correlated extremely well with theory for both average force and with theory for fold length. It will be covered in detail in Chapter Four.

1.2.4 Diverging Concertina Tearing

The emphasis of this research project was specifically diverging concertina tearing. It was found that once a tear began in the concertina mode from a pre-cut, it would begin

to diverge with a specified shape and would continue to diverge until the tears hit a boundary such as the previously mentioned vertical stiffeners. The diverging experiments in this paper were conducted on so-called infinite plates, in which the boundary conditions were far enough removed from the tearing that the clamping action of the frame could be ignored. The tests were limited by the stroke of the testing machine, and were not allowed to continue diverging until hitting the frame.

One shortcoming of all previous concertina tests was that in no case was the steady state process studied. Each study concentrated on the initiation of specific failure modes, but not on how the tearing proceeded. An additional goal of this project was to quickly attain steady state (by using a thin plate and small wedges) and studying the diverging shape and folding pattern.

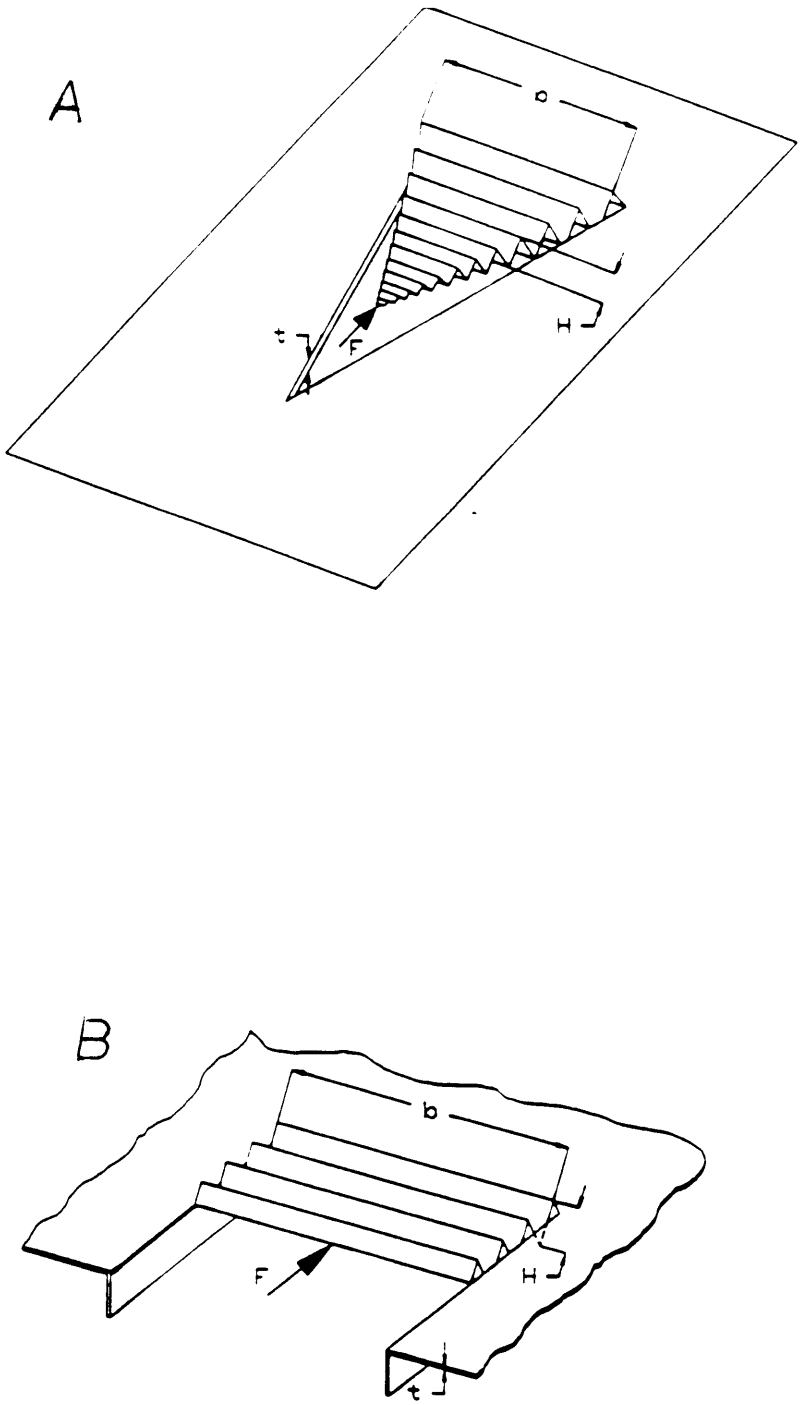

Fig. 1.1 Concertina Failure Diagrams

2 Experimental Procedures

2.1 Testing Facilities

All experiments were carried out on an Instron 20,000 lb_f screw driven universal testing machine. A 386 personal computer with a National Data Acquisition software package was used to process the output from the test machine, Figure 2.1. There was concern that the data acquisition program may not be set up properly or that there may be some problem with the machine since some of the output was showing cut off of the data peaks. It was recommended by Nurick [5] that a verification of the machine output be conducted.

The approach to verification was to conduct tensile tests on a 1000 lb_f Instron machine (that was known to give good results) and the 20,000 lb_f Instron machine, and then compare the results. To prepare the 20,000 lb_f Instron machine the connections between the data acquisition computer and the Instron were rewired, and the built-in chart recorder was returned to working order. The idea was to use the chart recorder from the 20,000 lb_f Instron machine and run the data acquisition program concurrently to ensure consistent output. Note that the rewiring was required because some of the connections were frayed. The rewiring cleared up the data cutoff problem.

The tensile specimens used were in accordance with ASTM section A370 specifications. Two tests were conducted on each Instron machine. There was excellent correlation of the force-displacement graphs between the 1000 lb_f Instron and the chart recorder output and data acquisition program output of the 20,000 lb_f Instron machine. The conclusion was that the setup and output of the 20,000 lb_f Instron machine was satisfactory and ready for testing.

2.2 Material Properties

The metal used in the experimental part of this study was ASTM A366 sheet metal in two thicknesses. For the infinite plate tests, samples with a thickness of 0.4 mm (0.016 inches) were used; for the longitudinally stiffened plate, a sample with a thickness of 1.130 mm was used. The infinite plate tests were conducted with the thinner plate and a small wedge to further lessen the edge effects of the clamped edges. For the stiffened plates, dimensions were used to create a scale model of a typical single hull VLCC.

An important material property for concertina tearing is the stress-strain relation. The material flow stress is the equilibrating variable in the mathematical relation between the force required to tear the sample and the displacement of the crosshead which allows this expression to be applied to different steels. The material flow stress must be calculated experimentally from the stress-strain curve.

The average flow stress is calculated from the stress-strain diagram. The ultimate stress, σ_{ult} is the stress level when the sample fails. The flow stress, σ_o is calculated by finding the stress required for 12% strain. Yield stress, σ_y is the stress level when the deformation ceases to follow the linear-elastic pattern and begins plastic deformation. In this test, the majority of the deformation is plastic, so it is necessary to calculate this value. The tensile tests were conducted following the guidelines of ASTM Specification A370.

Samples were machined from the steel per the dimensions of the ASTM specification. A dimensioned sketch of the sample is included as Figure 2.2. The samples were cut from an orientation of 0 and 90 degrees to the sheets rolling direction. Figure 2.3 illustrates the angle of orientation to the rolling axis. Note that a longitudinal

specimen corresponds to a roll angle of zero degrees. However, it was found that the results were essentially the same for each of the samples, whether they were from a 0^o or 90^o orientation.

A third important material property is the specific work of fracture, R, in Joules per unit area, Wierzbicki [6], Atkins [7] and Stronge et al [8]. This is a parameter characterization of the tearing process which assumes that the local deformation in the crack tip zone can be separated from the far-field processes. R is an experimentally determined value which is found through a long series of tests. For a mild steel, the range of values is

$$300\,N/mm \le R \le 1000\,N/mm$$

The specific work of fracture is related to the flow stress and two additional factors by

$$R = m\sigma_o\delta_t \qquad (1)$$

where δ_t is the crack opening displacement (COD) and m is a three-dimensionality factor.

2.3 Specimen Preparation

The specimens for the infinite plate tests were cut to dimensions of 16.5 inches by approximately 24 inches. In the tests begun from the free edge, the specimens needed to be shortened in order to fit the wedge above the edge of the sample due to the limited stroke of the testing machine. The tests from a precut hole were left the original size and were machined to accommodate the wedge. The longitudinally stiffened plate had the

same dimensions as the other plates which were initially cut from the free edge. Figure 2.4 shows the geometry of an unstiffened plate.

The unstiffened plates which had initiation on the free edge were simply notched the width of the wedge in the center of the plate, and the wedge was aligned with the notch. The wedge then pushed this tongue ahead as it formed the first fold. It was found, however, that the edge effects were too great, and concertina folding with a width b of the entire free surface began. This continued for about 10cm before a diverging pattern with an initial width equal to that of the wedge began.

The next set of tests was run with a precut hole slightly greater than the width of the wedge (b=9 mm for the small wedge tests, and b=20mm for the wide wedge tests). The hole began 20cm from the top of the plate and was approximately 20cm long.

The single hull longitudinally stiffened plate was precut by short slits at the inside edge of the welds for the stiffeners. This specimen also differed in thickness from the infinite plates. The specimen was designed to model a unidirectionally stiffened single hull VLCC. It was decided to scale the model by the stiffener/plate thickness ratio, using available thicknesses of ASTM A366 steel from stock. The end result was to use thickness t=1.130 mm for the plating and t= 1.829 mm for the flange. Figure 2.5 is the construction specifications for the longitudinally stiffened model.

2.4 Wedges, Adapter, and Frame Design

2.4.1 Wedges

There are as many possible wedge geometries as there are rocks in the ocean. Selecting the typical rock for use in modeling of wedge geometry is therefore not easy. The dilemma is to select a wedge geometry that makes analysis of the experiments easier, while trying to capture what happens in a real ship grounding.

Numerous wedges of various shapes and sizes have been designed and fabricated for the Tanker Safety Project experiments. For the concertina tests, the wedges can be categorized into small and large wedge sizes. The small wedges were designed for the first generation of load cell adapter and the wide wedge was designed for the redesigned load cell adapter. Each of the wedges was machined from solid blocks of cold rolled mild steel. Figure 2.6 shows the various sizes and tip shapes.

The small wedges have two different geometries. One is a square (blunt) end and has 90^{o} corners. The other small wedge is semicircular, with a radius equal to half the width of the wedge. The wide wedge has a wedge semi-angle of 45^{o} and the tip is rounded with radius r=1/16".

2.4.2 Adapter

Midway through this study, the testing apparatus was modified to accommodate the double hull tests. This section details the problem which was encountered and the solution to it. It was realized after the dramatic off-center loading observed in the double hull test that the same problem had existed for the single hull tests as well.

As the cutting of the first double hull specimen progressed to about two inches in depth, it was noticed that a significant moment was placed on the adapter connecting the wedge to the load cell. This adapter is approximately two feet in length. The cause of this was the frame holding the specimens had to be offset so that it could pass next to the adapter during the cutting stroke. The offset was on the order of three inches from the center of loading. The tremendous reaction force encountered in cutting both plates of the double hull specimen and this offset caused a moment to occur. The test was immediately stopped for fear of damaging the load cell. To correct this condition, a new adapter was designed consisting of four rods bolted to a plate. This plate was then connected to the load cell. This configuration allowed the specimens to be aligned directly under the center of loading and thus the rods would straddle the plate as the wedge progressed deep into the plate. Figures 2.7 and 2.8 show the side view of the load cell-to-wedge adapter configurations and a detailed wedge to adapter configuration.

2.4.3 Frame

The frame was designed by and constructed under the guidance of Maxwell. It was designed for forces exceeding those which occurred during the single plate tests of this study, so it is sufficient here to simple show the apparatus design figures [4]. Figures 2.9 through 2.11 show the frame design.

2.5 Test Parameters

The 20,000 kip Instron Universal Testing Machine has speed settings ranging from 2 inches per minute to 0.0002 inches per minute. Each crosshead speed was hand-timed and found to be correct, however this testing machine did not reliably run in the 2 inches per minute setting. Because of the need for the longest possible cut length in the tests (to allow time for steady state to develop), and because velocity is not important in the describing equations (as they are integrated over a time-like parameter and not time itself), the crosshead was run at the highest reliable testing speed, 1 inch per minute. However, after repairing the driver on the machine, one test was run under otherwise identical conditions with the wide wedge but at a testing speed of 2 inches per minute and the results were nearly identical. The velocity independence was also shown by the experimental team on a steady-state central cutting sample.

The load cell is an Instron 20,000 lb_f D30-20 load cell, with settings at 500, 1000, 2000, 5000, 10,000 and 20,000 lb_f settings. For each test, the highest expected load was estimated and the lowest possible load cell setting was used for highest resolution. The data acquisition program, National Data Acquisition NI-DAQ sampled voltages from the load cell at a rate of 40 samples per second and then averaged them for one data point per second. These voltages were then converted to forces using a Microsoft Excel spreadsheet and the calibration data from the Instron's built-in chart recorder.

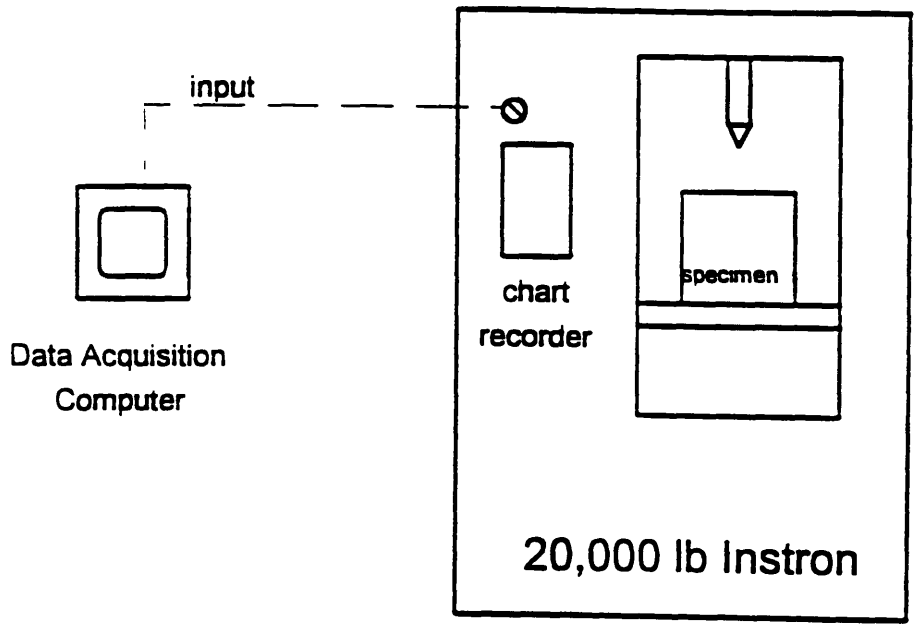

Figure 2.1 Schematic of 20,000 lb_f Instron Universal Test Machine and Data Acquisition System

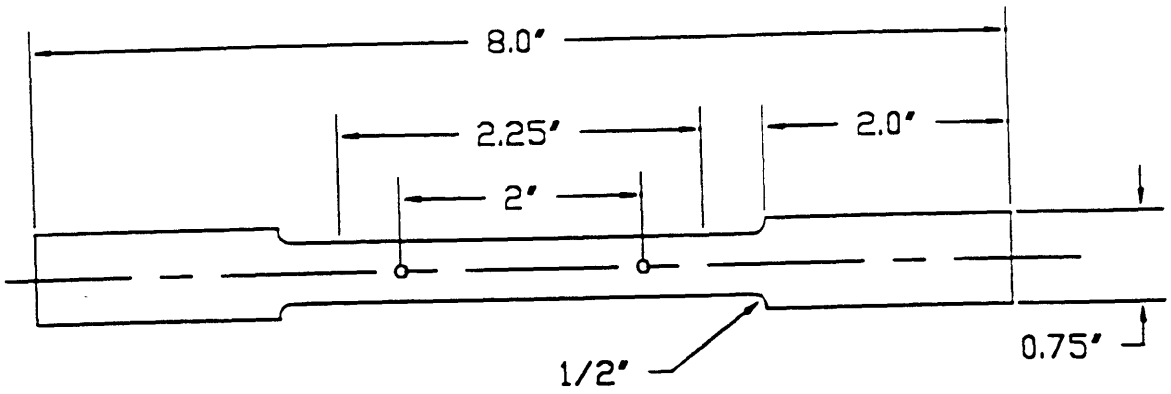

Fig. 2.2 ASTM A370 Flat Tensile Specimen

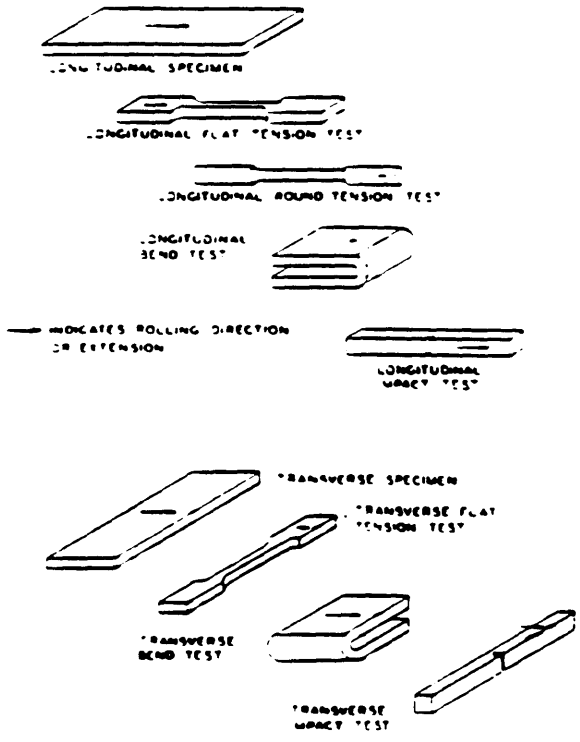

Fig. 2.3 Tensile Specimen Orientation

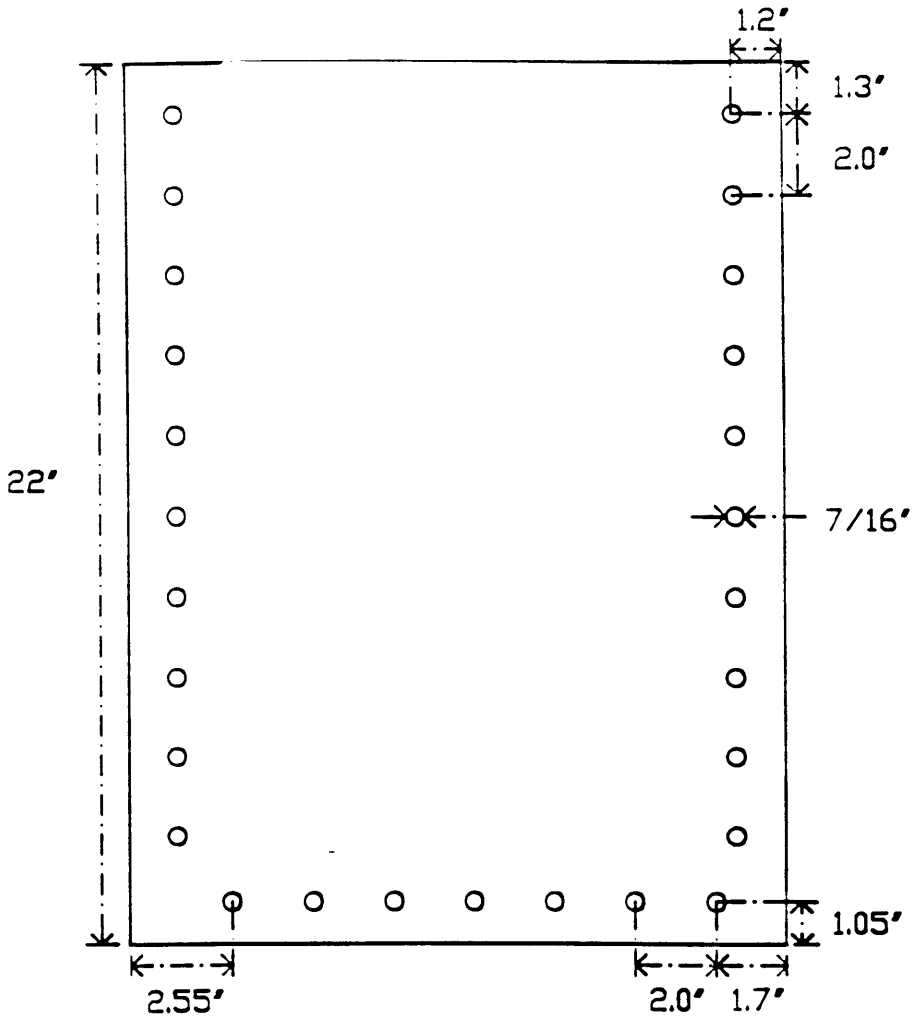

Figure 2.4 Geometry of Unstiffened Plate

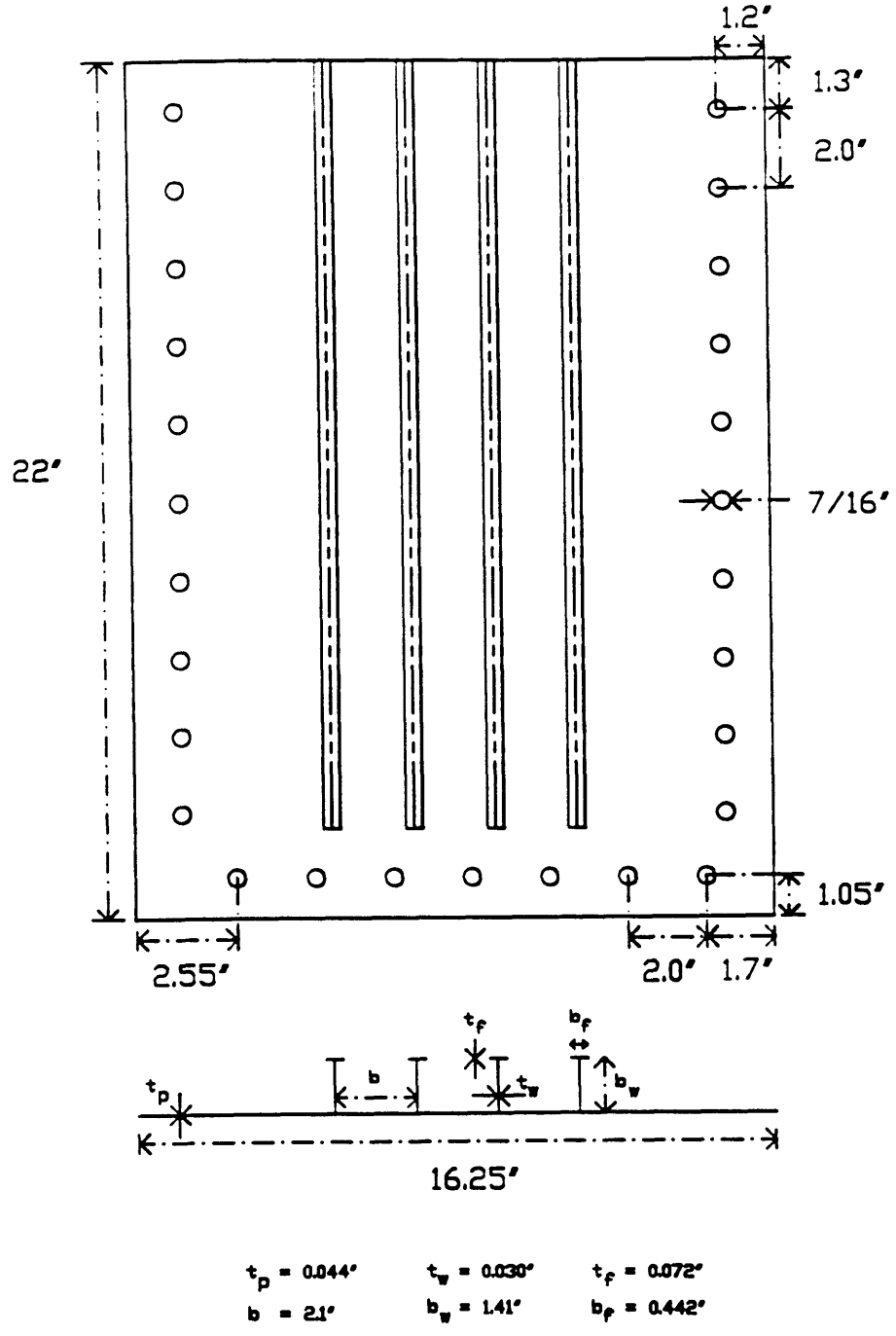

Figure 2.5 Longitudinally Stiffened Single Hull Model

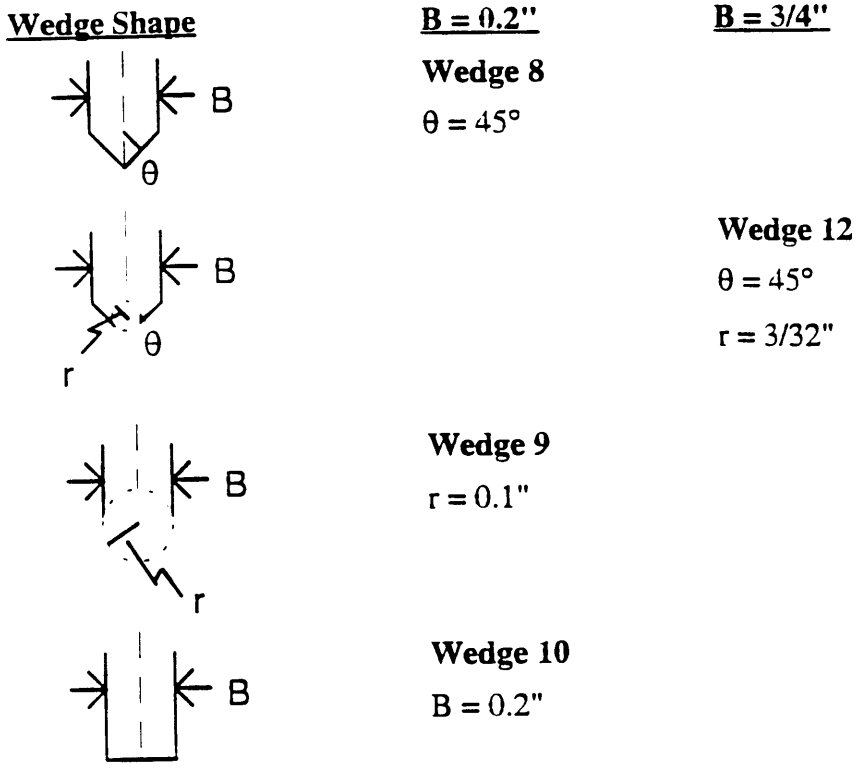

Fig. 2.6 Wedge Geometry

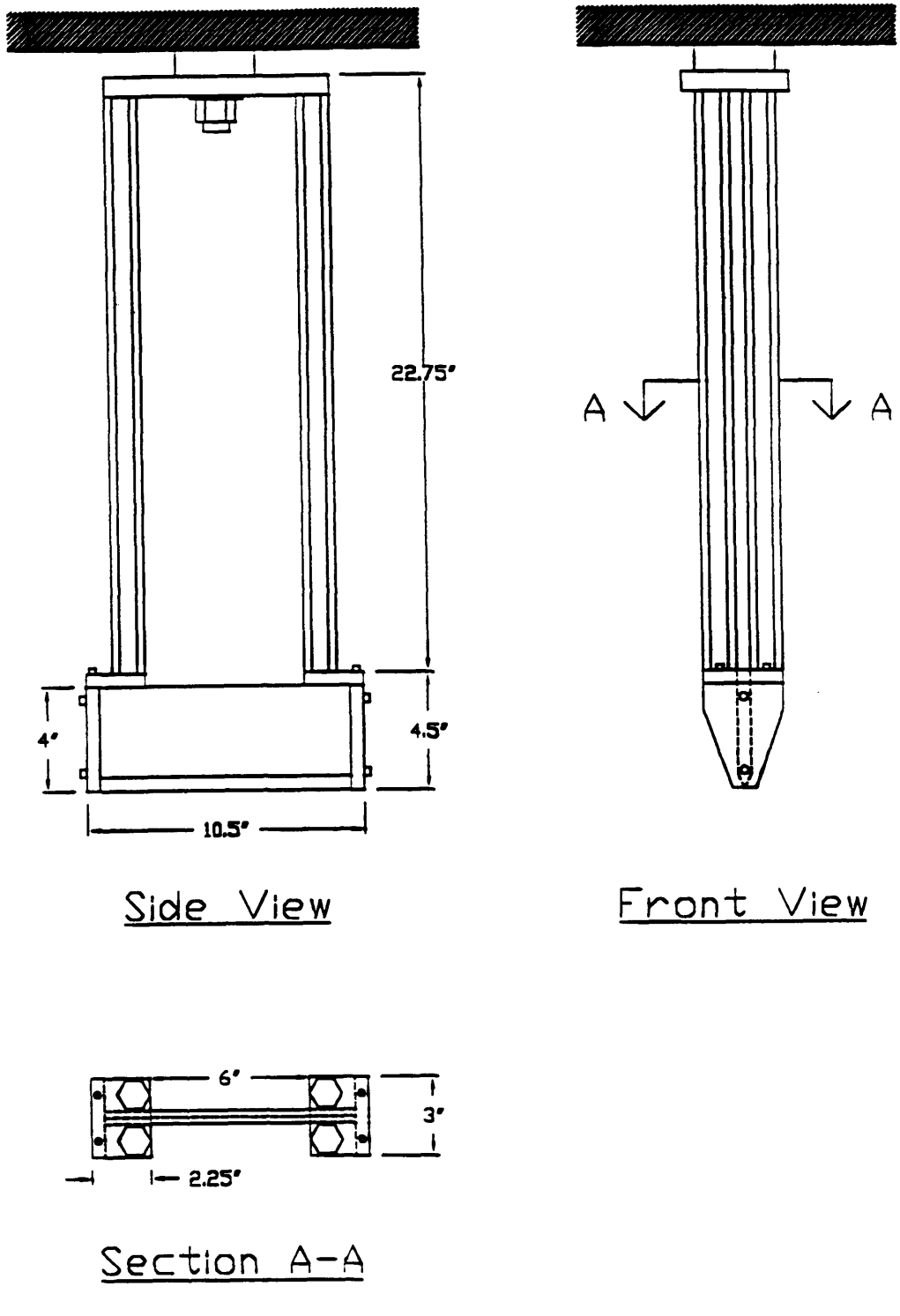

Figure 2.7 Side View of Load Cell-to-Wedge Adapter Configurations

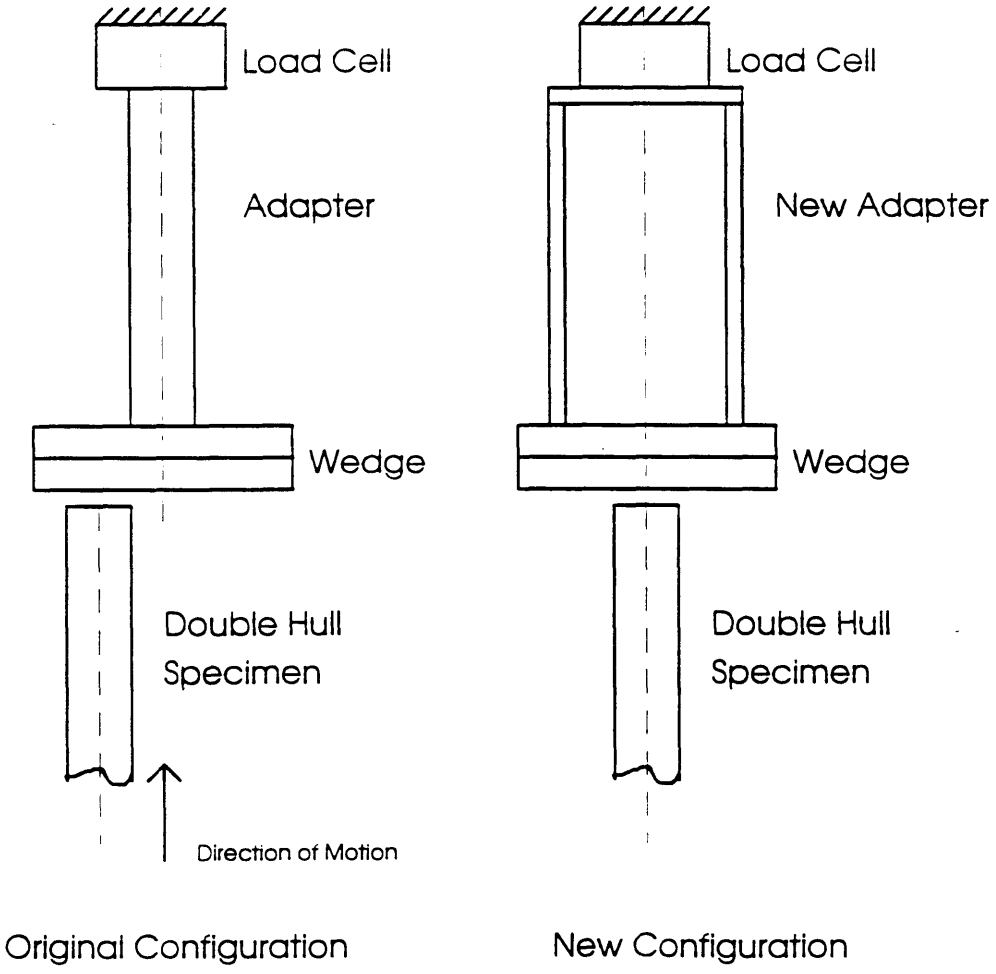

Figure 2.8 Modified Wedge Adapter Configuration

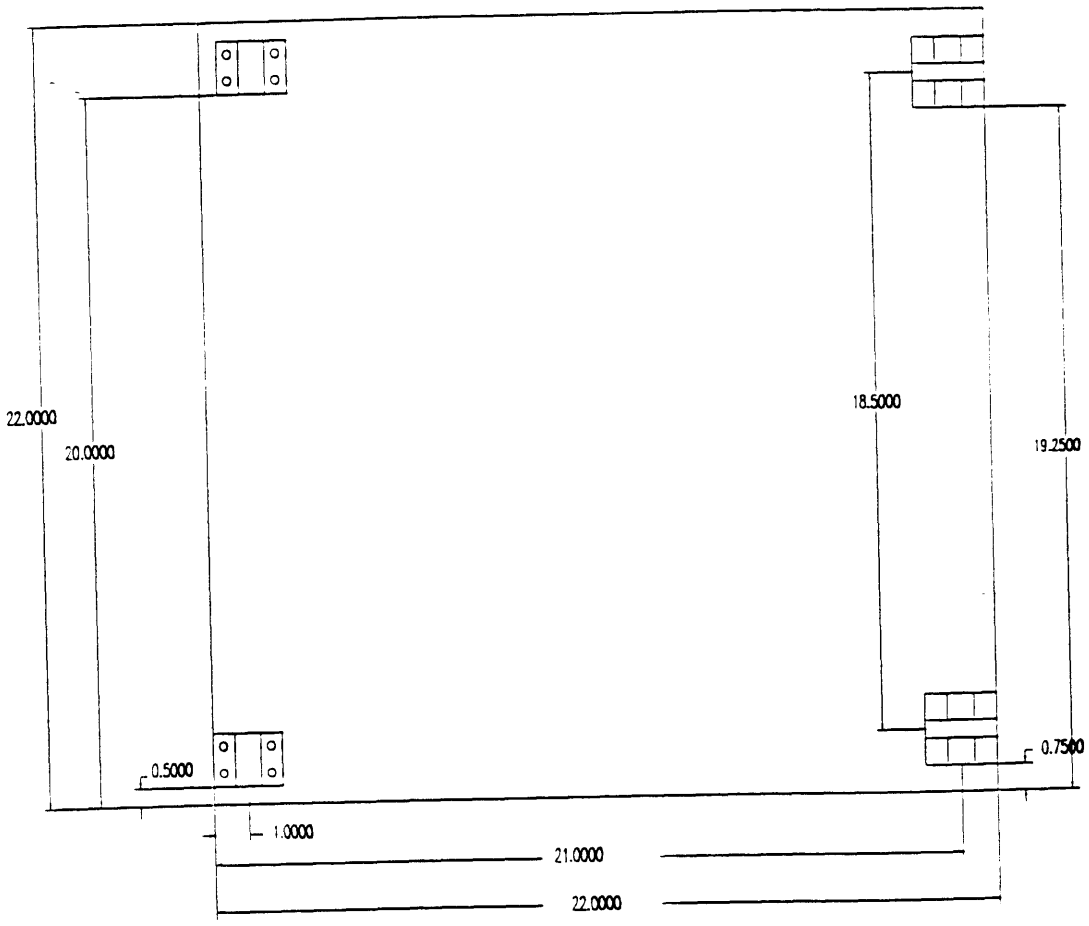

Figure 2.9 Base Plate Construction Drawing

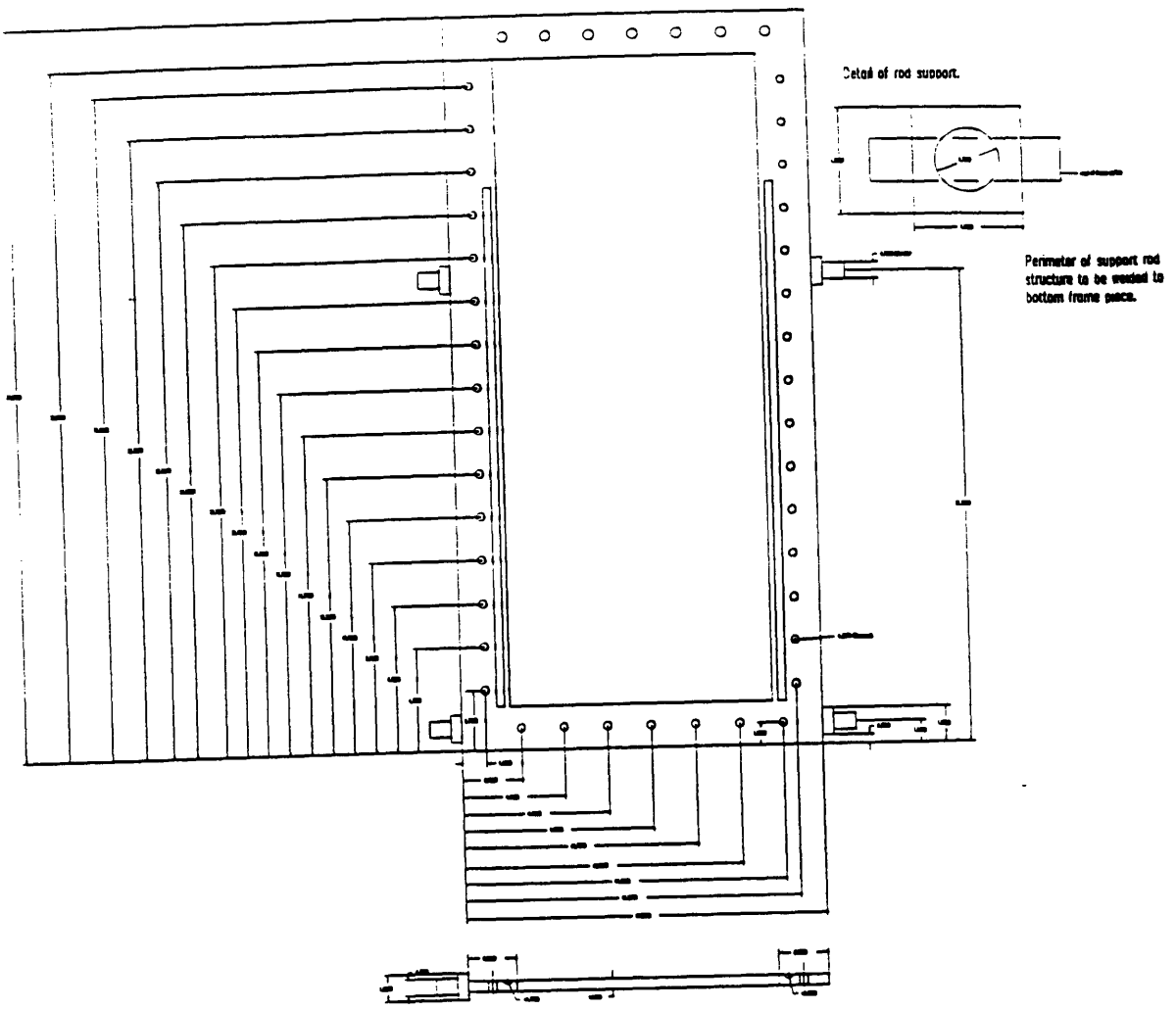

Figure 2.10 Frame Bottom Construction Diagram

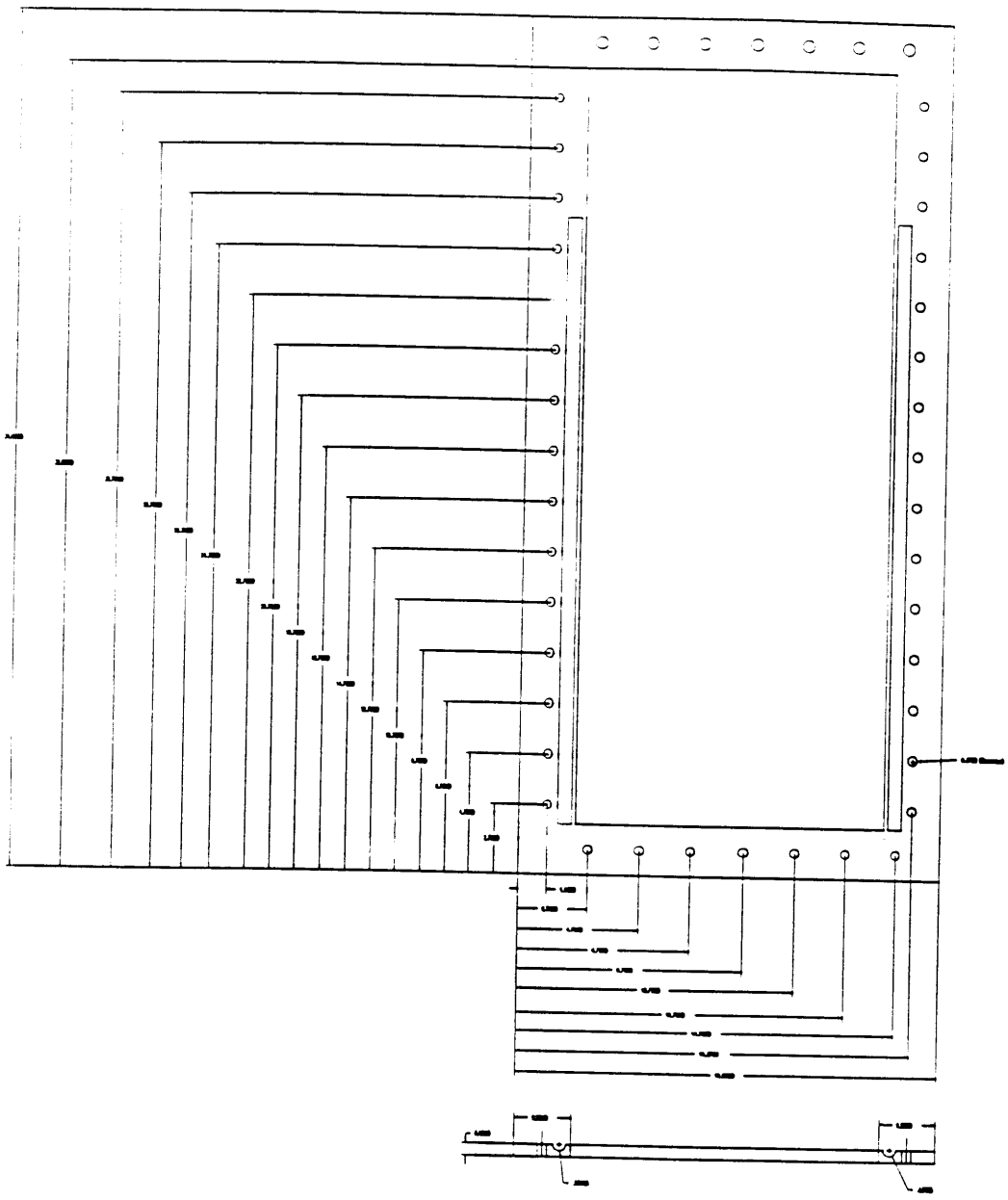

Figure 2.11 Frame Top Construction Diagram

3 Theory

This chapter will briefly outline the derivation of the theory for concertina tearing that Wierzbicki proposes in Report #22 of the Joint MIT-Industry Project of Tanker Safety, entitled "Concertina Tearing of Metal Plates: Improved Solution and Comparison with Experiments." An alternative to that solution proposed in Section 12 of the same report is also developed. Section 3.3 will then expand this theory to include diverging concertina and support the research conducted in this study.

3.1 Concertina Folding

The proposed mathematical model for concertina folding is based on the solution for progressive folding tubes, however that problem has been modeled with one fold being formed at a time. In the problem of concertina folding in sheet metal, qualitative tests show that the solution must include the interaction between two folding elements and not just one. Figure 3.1 shows a proposed model for this solution.

For a detailed description of the physical deformation pattern, the reader is referred to Wierzbicki [6]; however, a brief description will be given here. In the first phase (Fig. 3.1 (b)), a "roof" type mechanism is formed with stationary hinge lines and zones of in-plane compression in the transverse direction, which causes tearing fracture to occur at the support. This phase is completed when the back trapezoidal element and the front rectangular element first touch and are in a vertical position. The second phase is characterized by the rebending in which hinge lines and zones of in-plane compression in the transverse direction are formed within the trapezoidal element and a new "trapezoidal element" forms ahead of it. Thus, when a given element is in Phase I, there is always an

element in Phase II immediately preceding; conversely, there is always a Phase I element ahead of a Phase II element.

In order to find the folding wavelength, H, and the tearing force, F, we must start with the principle of virtual work. This will give the global equilibrium of the plate:

$$F\dot{u} = \dot{E}_b + \dot{E}_m + \dot{E}_s + \dot{E}_f \qquad (2)$$

where $\dot{u}$ is the wedge velocity, $\dot{E}_m$ is the rate of membrane energy, $\dot{E}_b$ is the rate of bending energy, $\dot{E}_s$ is the rate of shear energy, and $\dot{E}_f$ is the rate of tearing fracture energy. Since this is a periodic process and we are interested in the mean value for the resisting force, we can integrate Eq. (2) over a time-like parameter, i.e. τ being the time the wedge advances by $2H$.

$$\int_0^\tau F\dot{u}dt = \int_0^\tau \dot{E}_b dt + \int_0^\tau \dot{E}_m dt + \int_0^\tau \dot{E}_s dt + \int_0^\tau \dot{E}_f dt \qquad (3)$$

The next task is to calculate each of the terms in Eq. (3).

3.1.1 External Work

The left hand side of Eq. (3) must be evaluated by defining a relationship between force and displacement of the wedge:

$$E_{ext} = \int_0^\tau F(u)\dot{u}dt = \int_0^\tau F(u)du = F_m u\Big|_0^{2H} = F_m 2H \qquad (4)$$

where F_m is the mean force over the distance $2H$.

3.1.2 Energy dissipation due to bending

Following Wierzbicki [6], the bending energy is concentrated in a system of stationary hinge lines and no work is dissipated in the continuous bending mode, assuming fully plastic bending resistance. The rate of bending work in the i -th hinge line is equal to the product of the fully plastic bending moment M_o, the rate of hinge rotation $\dot{\phi}_i$, and the length of the hinge line l_i:

$$\left(\dot{E}\right)_i = M_o l_i \dot{\phi}_i \qquad (5)$$

Integrating Eq. (5) in time and summing over i , we get:

$$E_b = M_o \sum_i l_i \phi_i \qquad (6)$$

From the kinematic model proposed in Ref. [6], the total bending energy becomes:

$$E_b = 2\pi M_o \left[b + 2\xi\right] \qquad (7)$$

where

$$M_o = \frac{2}{4\sqrt{3}} \sigma_o t^2 \qquad (8)$$

3.1.3 Energy dissipated due to membrane forces

Following Wierzbicki [6], the rate of membrane work in the plane stress condition is:

$$\dot{E}_m = t\int_S \sigma_{\alpha\beta}\dot{\varepsilon}_{\alpha\beta}dS, \qquad \alpha,\beta = 1,2 \qquad (9)$$

It is assumed that the plate is inextensible in the x-direction, $\dot{\varepsilon}_{xx} = 0$, and that no work is done in shear deformation, $\dot{\varepsilon}_{xy} = 0$, so the only non-vanishing component of the strain rate is $\dot{\varepsilon}_{\xi\xi} = \dfrac{\partial \dot{u}_\xi}{\partial y}$. Integrating with respect to y gives:

$$\dot{E}_m = \frac{2}{\sqrt{3}}\sigma_o t\int_0^H \dot{u}_\xi d\eta \qquad (10)$$

where

$$\dot{u}(\eta) = \dot{\Delta}\frac{\eta}{H} \qquad (11)$$

is the velocity component in the y-direction and $\dot{\Delta}$ is the maximum tip velocity difference at the transverse edge of the plate. After substitution and integration with respect to time, the kinematic model developed in Ref. [6] gives:

$$E_m = \frac{1}{\sqrt{3}}\sigma_o \frac{H^3}{\xi}t \qquad (12)$$

3.1.4 Energy Dissipated in Shear

There is a relative shear displacement between the shared boundaries of each folding element. This displacement causes a shear strain in the back rectangular element of area $S = \xi\eta$. The rate of shear energy for one side is:

$$\dot{E}_{sh1} = \frac{\sigma_o}{\sqrt{3}} t \int_S 2\dot{\varepsilon}_{\xi\eta} dS \qquad (13)$$

According to Ref [6], this becomes:

$$E_{sh1} = \frac{1}{2} M_o \frac{H^2}{t} \qquad (14)$$

This value must be doubled, then, because there is an identical element on either side of the symmetry line; it must be doubled again due to shear strain reversal. Thus the total energy dissipated in shear is:

$$E_{sh} = 4E_{sh1} = 2M_o \frac{H^2}{t} \qquad (15)$$

3.1.5 Energy Due to Tearing

The energy due to tearing was derived in Ref. [6] directly from the COD (Crack Opening Displacement) criterion. Defining δ_t as the Crack Tip Opening Displacement (CTOD) parameter and neglecting as before the effect of shear, the tearing energy is:

$$E_f = \int \dot{E}_m dt = \frac{2}{\sqrt{3}} \sigma_o t \int_0^{2H} d\eta \int_0^{\delta_t} du = \frac{2}{\sqrt{3}} \sigma_o t \delta_t 2H \qquad (16)$$

3.1.6 Folding wavelength

Combining the external work, the energy dissipation due to bending, the energy dissipation due to membrane forces, the energy dissipated in shear, and the energy dissipation due to tearing, gives:

$$\frac{F_m}{M_o} = \pi \frac{b}{H} + 2\pi \frac{\xi}{H} + \frac{H^2}{\xi t} + 2\frac{H^2}{t} + 4\sqrt{3} m \frac{\delta_t}{t} \qquad (17)$$

Minimizing the mean indentation force with respect to H and ξ gives two algebraic equations:

$$\frac{1}{t} + \frac{2H}{\xi t} - \frac{\pi}{H^2}(b + 2\xi) = 0 \qquad (18)$$

$$\frac{2\pi}{H} - \frac{H^2}{\xi^2 t} = 0$$

These equations can only be solved in an approximate way and lead to

$$\frac{H}{t} = \left(\frac{b}{t}\right)^{0.57} \qquad (19)$$

$$\frac{\xi}{t} = 0.4\left(\frac{b}{t}\right)^{0.855}$$

3.1.7 Mean Indentation Force

Substituting these optimum values for H and ξ into the equation for mean indentation force and taking $m = \sqrt{3}$ gives the mean indentation force for non-diverging concertina to be

$$F_m = 3\sigma_o t^{5/3} b^{1/3} + 2\sqrt{3} t \sigma_o \delta_t \qquad (20)$$

3.2 Alternative Solution

Wierzbicki [6] suggested that although not as rigorous of a solution, an alternative way to accommodate the relative displacement is to compress the deformed shape *GMN* and make it compatible with *C'D'G'*. This solution leads to much simpler algebra, as the optimization of H and ξ can be solved directly. The energy dissipation due to shear should be replaced by the membrane tension/compression energy. Figure 3.1 shows the interaction between these elements.

This gives us the non-dimensional mean force equation, in terms of H and ξ .

$$\frac{F_m}{M_o} = \pi\frac{b}{H} + 2\pi\frac{\xi}{H} + 2\frac{H^2}{\xi t} \qquad (21)$$

A minimization with respect to H and ξ occurs at

$$H = 0.56b^{2/3}t^{1/3} \qquad \xi = b/6 \qquad (22)$$

Giving us the optimum mean force F_m

$$F_m = 3.25\sigma_o t^{5/3} b^{1/3} + 2Rt \qquad (23)$$

3.3 Diverging Concertina

The solution for concertina tearing is assuming a plate of thickness t, with flow stress σ_o, and a constant tear width b. For diverging concertina tearing, however, it is not possible to simple assign a constant value to the tear width b. The solution to this problem lies in finding the diverging shape that the deformation follows. In this discussion, it is presented that the tearing occurs orthogonally to the direction of the principal stress, i.e. the tear is orthogonal to the segment (modeled as a straight line) which runs from the tip of the wedge to the point of tearing, Figure 3.2. From geometry, a differential equation governing the tearing shape can be derived.

$$\frac{dy}{dx} = \frac{H}{y} \qquad (24)$$

where H is given by Eq. (22).

$$b = 2y \qquad \frac{dy}{dx} = \frac{0.56(2y)^{2/3}t^{1/3}}{y} \qquad (25)$$

In terms of non-dimensional quantities, $\bar{y} = \frac{y}{t}$, $\bar{x} = \frac{x}{t}$, and initial tear width, $\bar{y}_o = \frac{y_o}{t}$, Eq (25) becomes:

$$\frac{d\bar{y}}{d\bar{x}} = 1.58\frac{0.56}{\bar{y}^{1/3}} \qquad (26)$$

Separating this ODE, and integrating gives the tear width $\bar{y}$ with respect to non-dimensional cut length $\bar{x}$ and using the initial condition $\bar{y}(\bar{x} = \bar{x}_o) = \bar{y}_o$ gives:

$$\bar{b} = 2\bar{y} = 2\left(1.179\bar{x} + \bar{y}_o^{4/3}\right)^{3/4} \qquad (27)$$

where $\bar{y}_o$ is the dimensionless initial width of the tear (pre-cut). Substitution of this into Eq. (22) gives us a final relation between cut length, initial tear width, and the mean indentation force:

$$F_m = 4.09\sigma_o t^2\left[1.179\bar{x} + (\bar{y}_o)^{4/3}\right]^{1/3} + 2Rt \qquad (28)$$

3.4 Thick Plate Solution

The solution for concertina folding so far has been based on the assumption that the folding is linear, such that the folding distance is the entire length of the folding element, $2H$. However, in tests conducted on thicker plates, it was observed that the folds were not constructed of straight segments, but rather they were a series of connected circular sections. Thus, according to Wierzbicki and Abramowicz [6] and [9], the effective crush distance is equal to approximately 75% of the available crush distance.

This causes the equation for the mean indentation force to increase by a factor of 4/3. Figure 3.3 shows these cross-sectional shapes.

$$F_m = 4.33\sigma_o t^{5/3} b^{1/3} + 2Rt \qquad (29)$$

The diverging solution is then

$$F_m = 5.45\sigma_o t^2 \left[1.179\bar{x} + (\bar{y}_o)^{4/3}\right]^{1/4} \qquad (30)$$

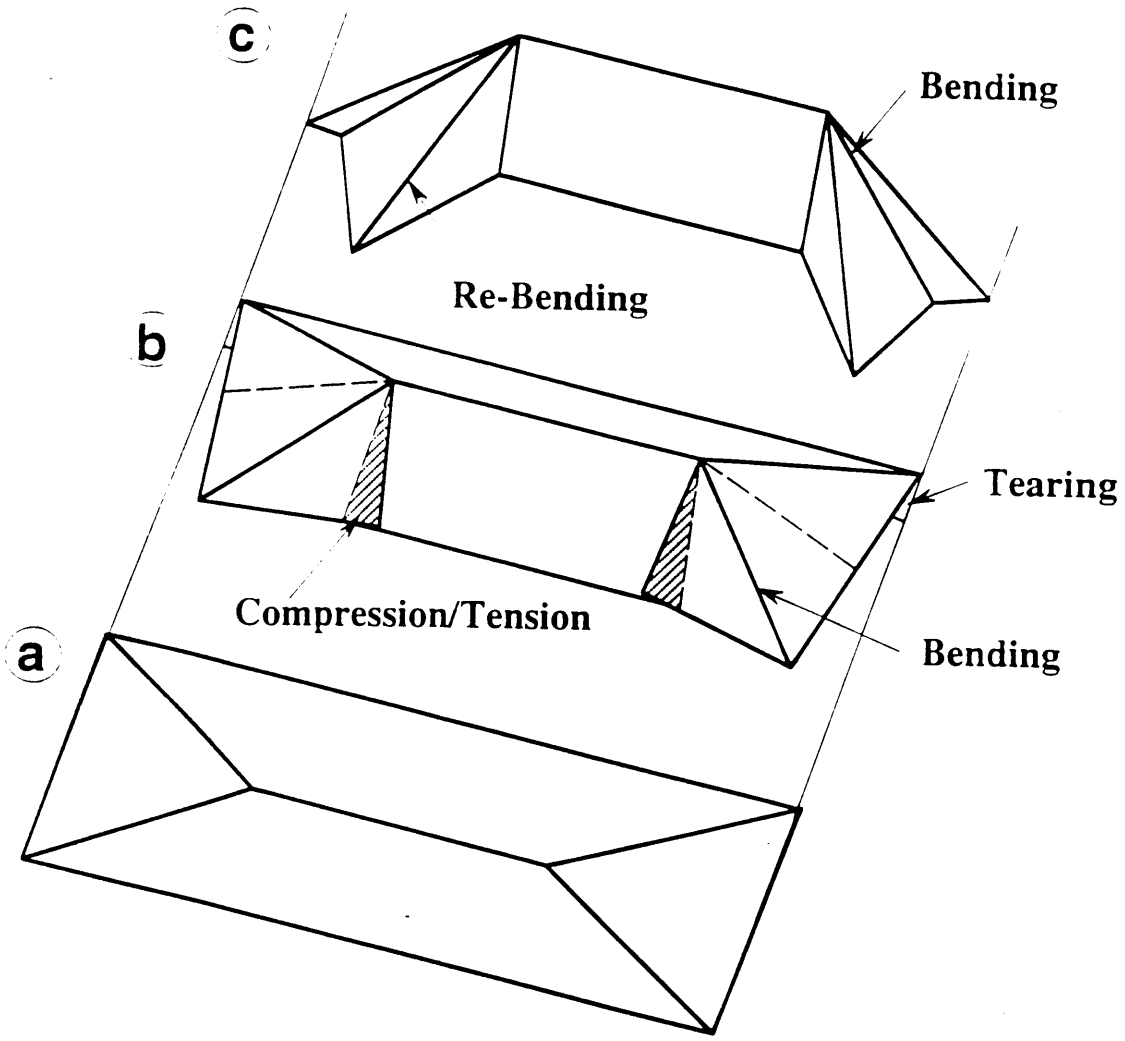

Figure 3.1 A two stage computational model of concertina tearing. Undeformed plate (a). Bending, compression/tension and tearing (b). Bending and rebending (c). [6]

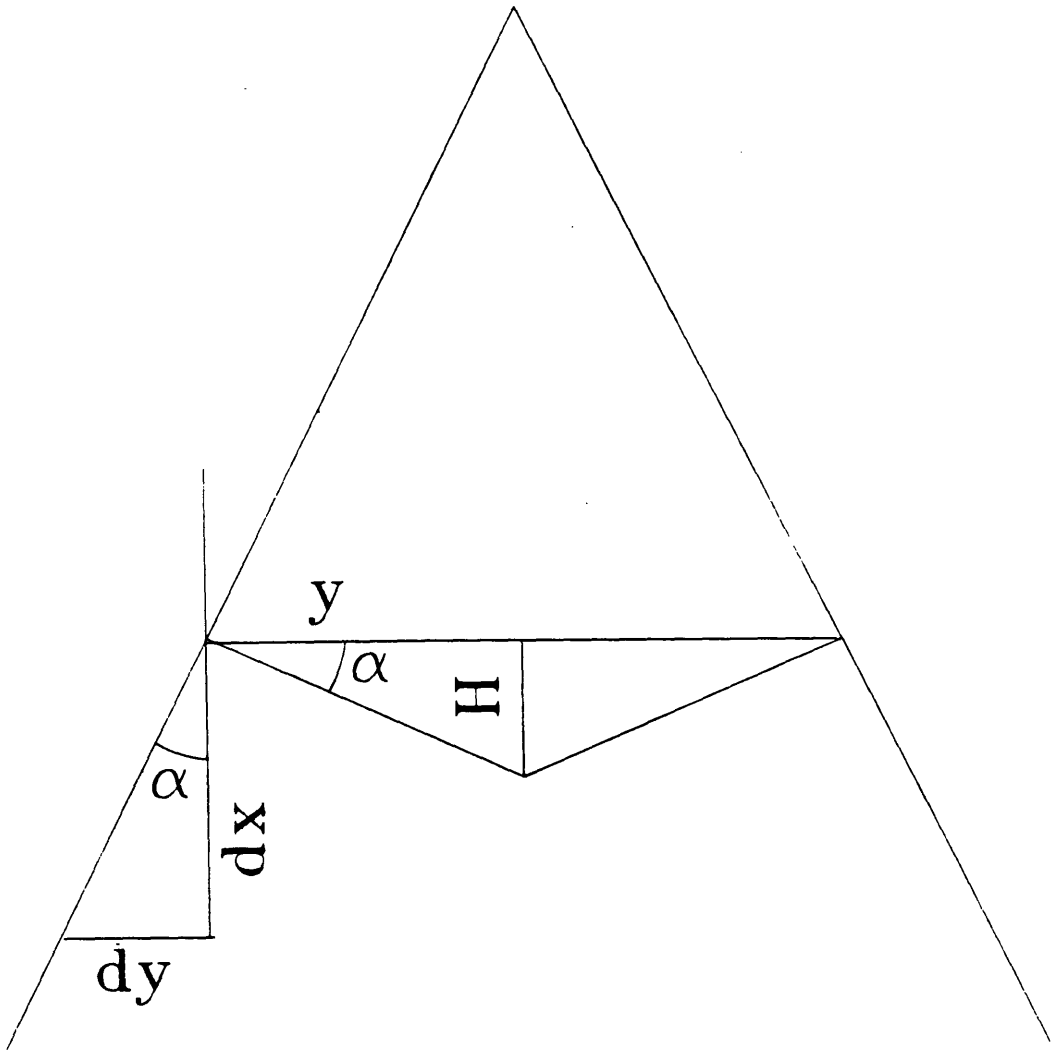

Figure 3.2 Geometry of Diverging Concertina

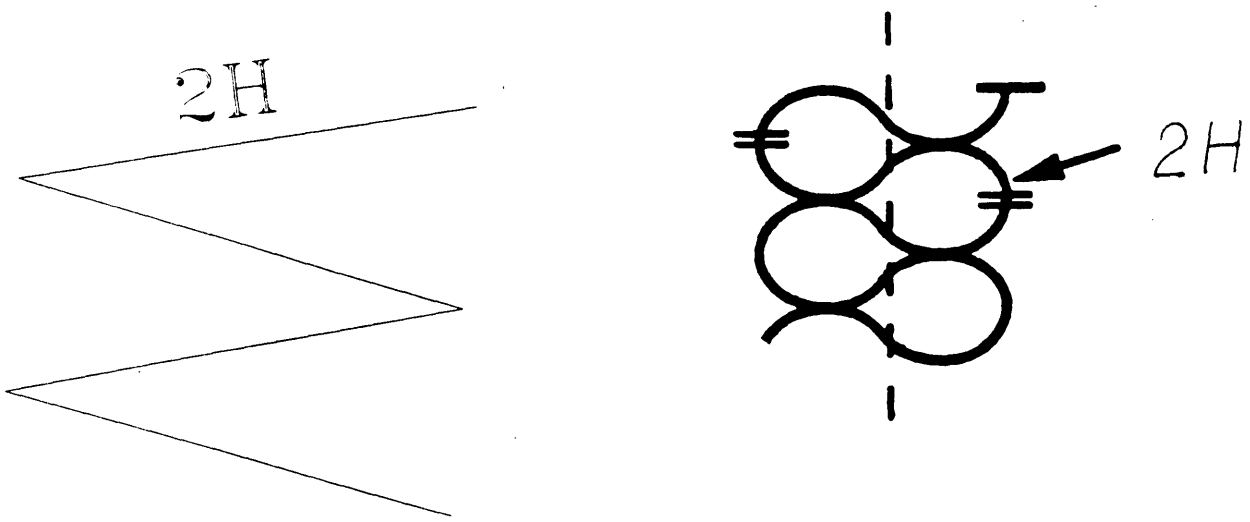

Figure 3.3 Diagram of available (a) and effective (b) crush distance.

4 Experimental Results and Discussion

In each test, the specimens were sheet steel, ASTM A366, and had a plate thickness, t, equal to 0.4 mm. Table 1.1 gives a summary of the qualitative test results. It is shown that there is good repeatability in failure mode from each set of experimental parameters. It is important to note that parameters such as material, deformation speed, angle of attack, and thickness remain constant throughout the tests. A detailed account of the experiments follows.

Test Number	Wedge Shape	Wedge Width	Initiation Type	Crosshead Velocity	Failure Mode
1	Blunt	0.2 in	Free Edge	1 in/min	Concertina
2	Blunt	0.2 in	Free Edge	1 in/min	Concertina
3	Blunt	0.2 in	Precut Hole	1 in/min	Concertina
4	Blunt	0.2 in	Precut Hole	1 in/min	Concertina
5	Rounded	0.2 in	Precut Hole	1 in/min	Concertina
6	Rounded	0.2 in	Precut Hole	1 in/min	2-Mode
7	Rounded	0.2 in	Precut Hole	1 in/min	2-Mode
8	45^{o} Rounded	0.75 in	Precut Hole	2 in/min	Concertina
9	45^{o} Rounded	0.75 in	Precut Hole	1 in/min	Concertina
10	45^{o} Rounded	0.75 in	Free Edge	1 in/min	Bounded

Table 4.1 Summary of Experimental Results

The first four tests were conducted with a narrow square wedge. Although the tests were initiated differently (two from the free edge, and two from a precut hole inset from the edge) each test clearly demonstrated a diverging concertina mode of failure. The next three tests were also conducted using a narrow wedge, this time with a semi-circular cross section. The first test behaved very similarly to the blunt wedge, with regular diverging concertina. The second and third tests had a slight induced eccentricity and alternated modes between a diverging concertina and a pure cutting. The third type of test was conducted with a wider wedge. This wedge had a 45^{o} wedge semi-angle, and a rounded tip, r=1/16". These tests were expected to also cause a two mode deformation. However, even with an exaggerated eccentricity (approximately 10 degrees from orthogonal) only diverging concertina tearing occurred. One of these tests was run with a crosshead velocity of twice the other tests to show the velocity independence of the mean indentation force. The fourth type of test was run on a longitudinally stiffened single hull panel. This sample was precut at the welds to immediately initiate bounded concertina and not "waste" crosshead stroke to attain steady state.

4.1 Narrow Wedges

The first tests were conducted using wedges with a width of 0.2 inches. The narrow wedge was modeled after a pencil eraser which was used on Xerox paper tearing tests, [10].

4.1.1 Tests Initiated from Plate Edge

The first two tests were precut at the free edge such that the precuts were centered on the wedge and there 9 mm wide. In both cases, as the wedge began cutting the sample, only one side of the cut continued to form. A part of the plate on the other side of the

wedge began concertina folding which extended all the way to the support frame. This continued for approximately 60 mm while the single tear migrated under the center of the wedge. As the membrane tension increased, the mode of failure changed. The samples "bunched up" immediately before the wedge and began a clear concertina tearing mode Figure 4.1 is a photograph taken of the sample after failure from where the concertina mode began in sample #1. Figure 4.2 is a photograph of test #2 and shows the characteristic wavy plastic deformation along the length of the tears. and the accordion-folded steel which was pushed before the wedge.

The graph of force vs. displacement (cut length) shows the sinusoidal shape of the force for test #1, Figure 4.3. The plot for test #2 is shown as Figure 4.4. As the metal bends, the force increases until the peaks represent the instant before the tearing began. The force decreases while the specimen tears, and then begins to increase as the specimen folds again. The average value of the sinusiod increases as the cut length increases because the tear width also increases.

The graph of wavelength, H, vs. cut width, b, shows that the wavelength does grow almost as predicted, Figure 4.5. Also shown is a diagram for the diverging shape of tests #1 and #2 in Figures 4.6 and 4.7. These figures show that the predicted shape is very accurate.

4.1.2 Tests Initiated from Precut Hole

The third through seventh tests were initiated by inserting the narrow wedge into a precut hole with width 9 mm in the samples. The notches were cut approximately 20 cm from the top edge to avoid the effect of free edge boundary conditions. All of the tests began immediately with the concertina tearing mode.

Square Wedge

The third test did not deform straight along the axis of motion of the wedge. Either because the precut was not straight of the wedge was not aligned perfectly in the center of the notch, the tearing skewed to the side. (Figure 4.8) The fourth tests developed into a textbook example of concertina tearing mode, with the initial tear width known and perfectly symmetric geometry. (Figure 4.9)

The force-displacement graph and wavelength-tear width data for test #3 show that, although the geometry was skewed, there is still good correlation between the experimental data and the theory. The force-displacement curves for tests #3 and #4 are included as Figures 4.10 and 4.11.

The wavelength data for both tests is displayed in Figure 4.12 and compared with the prediction of Eq. (22). The correlation is very good for approximately the first 15 cm of the wedge travel and then degenerates. Figures 4.13 and 4.14 show the diverging tear width with respect to the cut length for tests #3 and #4. In test #3, note that although the test skewed to the side, the cut width still diverged as Eq. (27) describes.

Round Wedge

The first test conducted with the narrow round wedge is indiscernible in both qualitative and quantitative measures from the square wedge tests initiated from a precut hole. The test again began immediately with concertina tearing. It entered into a diverging mode and followed the predicted shape closely. The mean indentation force level was slightly less than the predicted range until the 0.15 meter cut length, but the

force increased to the mean level by the end of the test. The folding wavelength was very similar to what was expected. Figures 4.15 through 4.18 show the deformed specimen and correlation with the theoretical predictions.

Tests #6 and #7 were also run with the narrow round wedge initiated from a precut hole; however, in these tests a slight eccentricity was introduced. The wedge was aligned slightly askew from orthogonal to the plate, simulating more realistically the non-idealness of an actual VLCC grounding scenario. Physical observation of a grounded ship in dry-dock showed the alternation between modes in a full-scale scenario, validating this experimental model. In the tests, the wedge began concertina tearing as in the previous tests, but as these experiments progressed, the concertina folds began to be pushed off to the side. Rather than stop the test, each sample was allowed to continue. One tear eventually migrated beneath the wedge as the fold was pushed completely off to the side; central cutting began from this tear.

After the central cutting progressed for a brief period, approximately 5 cm in test 6, and seven centimeters in test #7, the metal again bunched up before the wedge and began diverging concertina. It was noticed that the mean force level for both the central cutting (Zheng and Wierzbicki [11]) and the force level at the re-initiation of concertina tearing remained almost constant in both tests. Figures 4.19 and 4.20 show the torn specimens, and Figures 4.21 and 4.22 show the correlation with mean force predictions for both concertina and central separation.

4.2 Wide Wedge

The wide wedge, described in section 2.4.1, was initially expected to also show a multiple mode deformation, and was thus set with an initial eccentricity. However,

because of the wedge shape, the concertina folds were "caught" and the wedge and not pushed clear of the wedge in the test #8. The folds were beginning to skew to the side at the cut length that the test was stopped due to the limited stroke of the Instron UTM, and given sufficient testing length would eventually have entered into central cutting.

Test #9 was run at a crosshead speed of two inches per minute. This was done to show the velocity independence of concertina tearing. Again, pure diverging concertina tearing occurred, with mean forces and geometries following almost exactly the predicted values. Similarly to the independence on round vs. blunt narrow wedge geometry on the failure process, it is virtually impossible to tell the one inch per minute test from the two inches per minute test by qualitative or quantitative means. Figures 4.23 through 4.29 show photographs of the specimens #8 and #9 and also show the correlation with predicted mean indentation force levels, diverging shape, and cut width vs. fold length.

4.3 Bounded Concertina Tearing

One final type of concertina tearing is folding which occurs between two solid boundaries. In the early concertina initiation tests by Maxwell [4], these boundaries were the frame supports. In test #10, the boundaries are longitudinal stiffeners which are electron beam welded to the plate. This test was conducted using the wide wedge at a crosshead velocity of one inch per minute. The base plate in this test was a thicker sample than the other experiments in this study, and is more accurately described by the thick plate equations, Eq. (29). The sample was initially precut from the free edge at the vertical stiffeners to ensure initiation in bounded concertina, and not initially diverging until ultimately reaching the stiffeners. The folds occurred in a very regular pattern, with the folding wavelength effectively constant over the entire test, and nearly equaling the expected value. The measured folding wavelength is 7.37mm and the predicted value is

7.87mm, giving an error of only 6.3%. Figure 4.30 shows the deformed specimen, with regular folds between the stiffeners, and Figure 4.31 show the correlation with the predicted mean force level.

Figure 4.3 Test #1: Comparison of measured and predicted force-displacement relationship

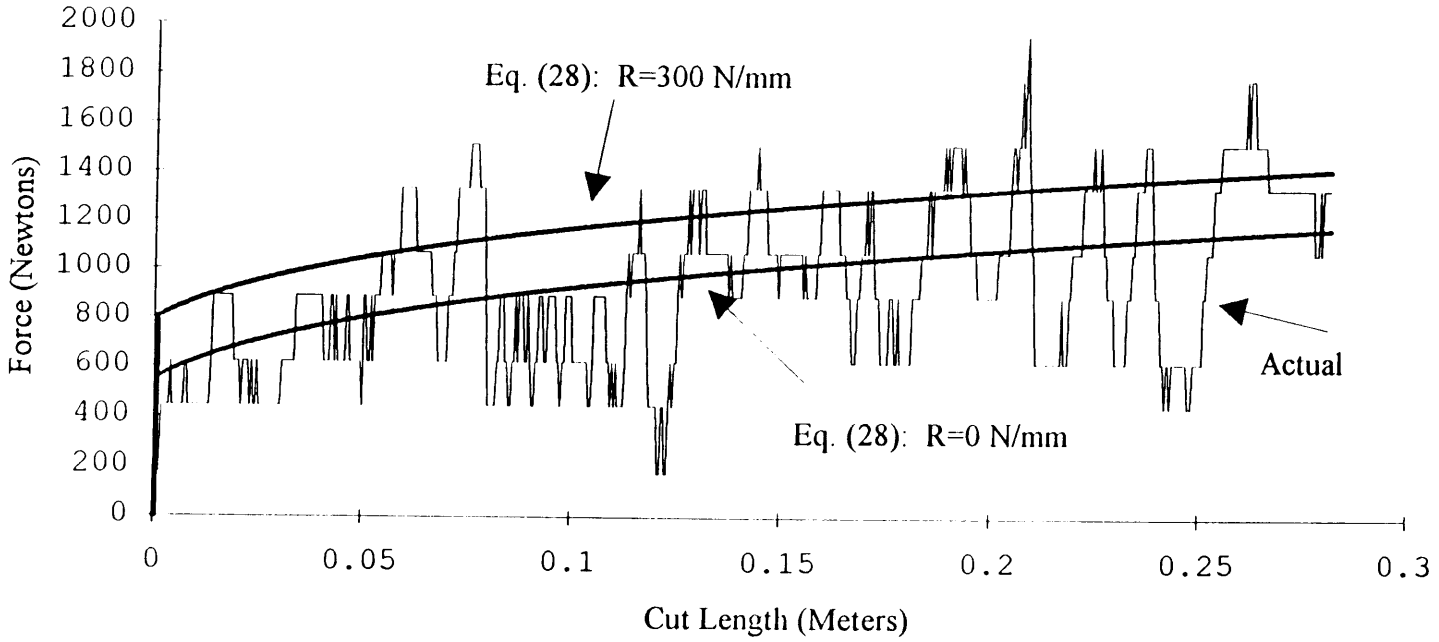

Figure 4.4 Test #2: Comparison of measured and predicted force-displacement relationship

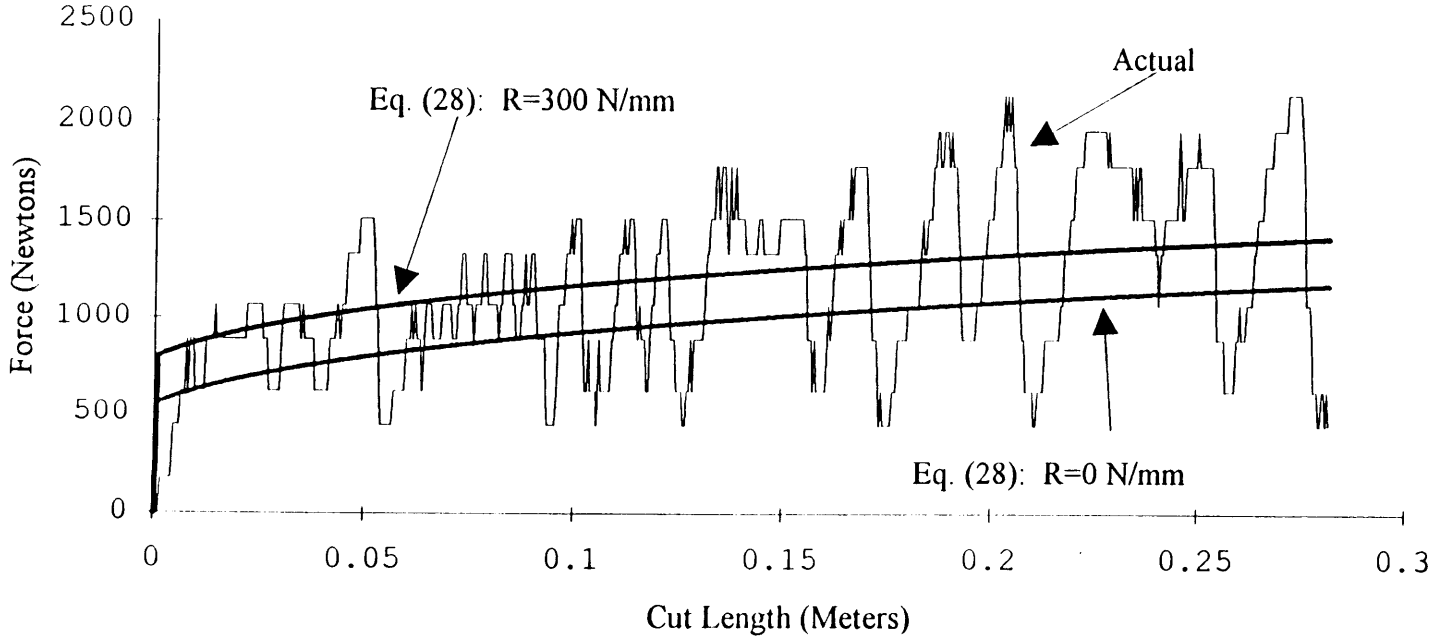

Figure 4.5 Comparison of wavelength vs. cut width in tests #1 and #2

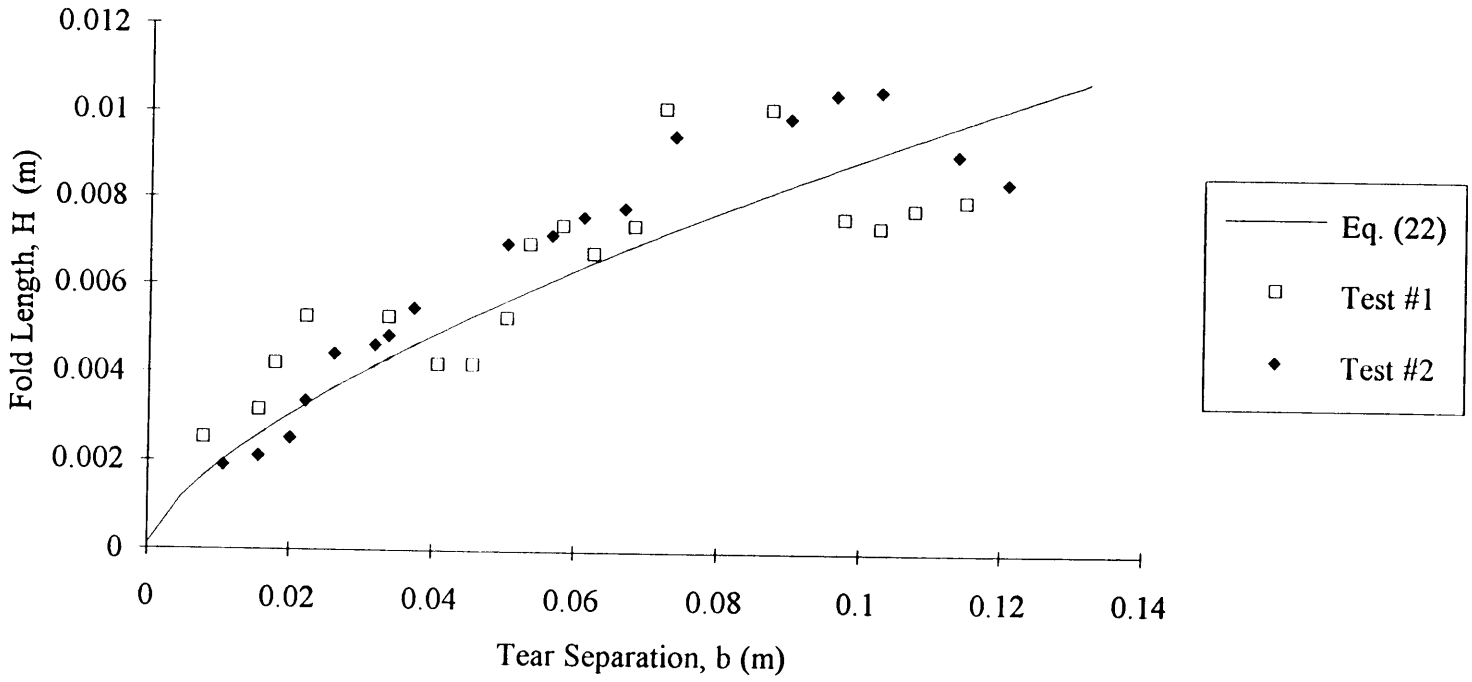

Figure 4.6 Diagram of diverging geometry in test #1

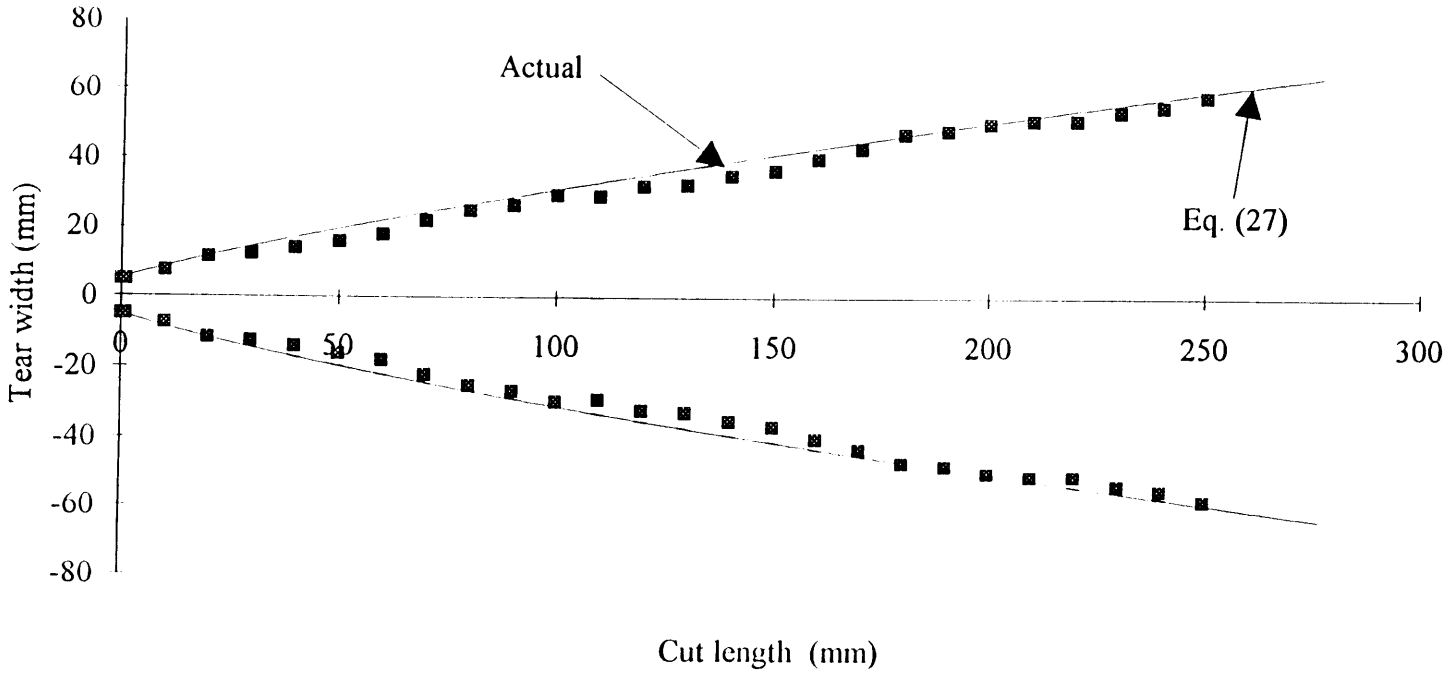

Figure 4.7 Diagram of diverging shape in test #2

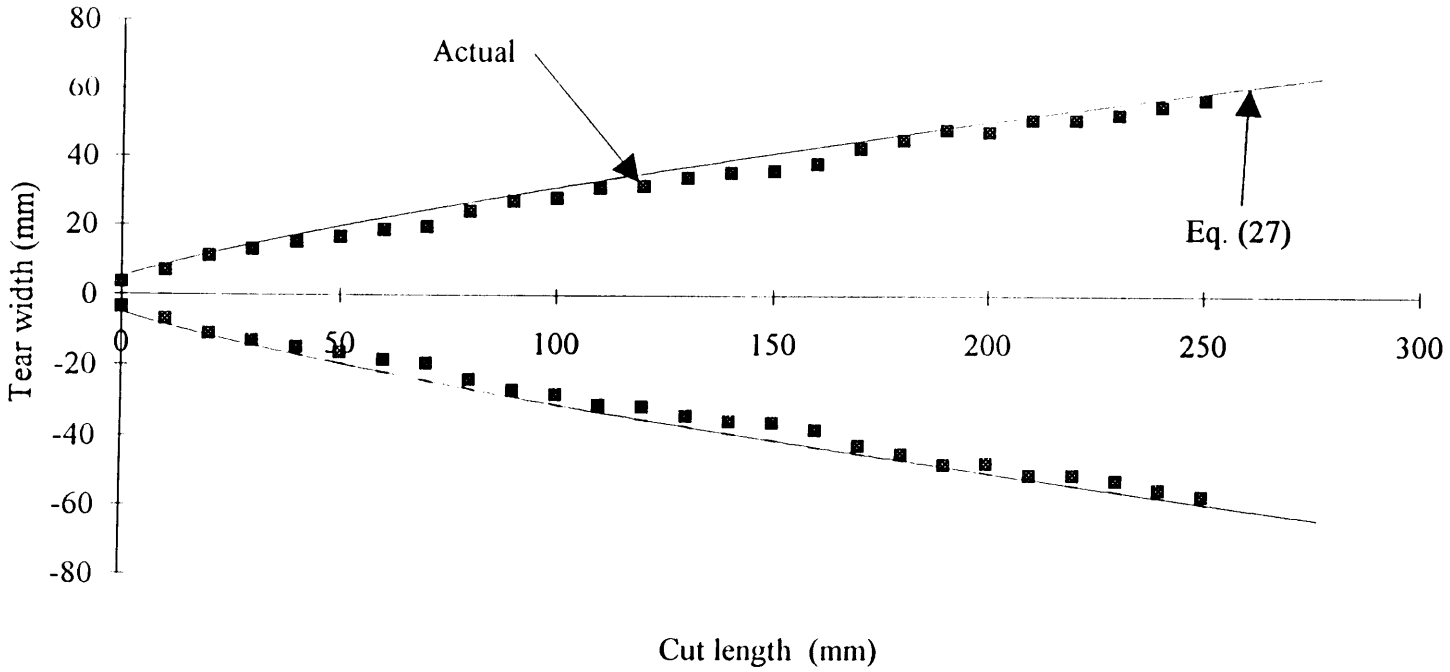

Figure 4.8 A photograph of the deformed specimen #3 at the end of the test.

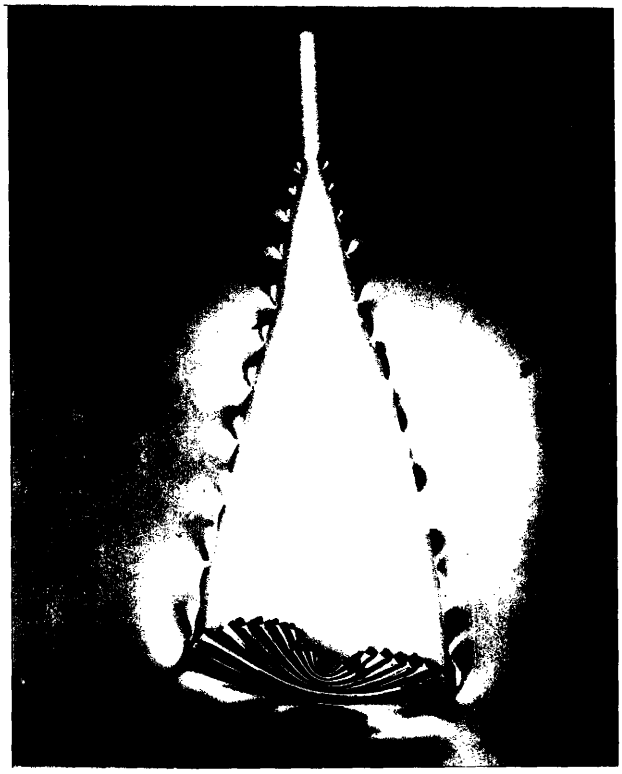

Figure 4.9 A photograph of the deformed specimen #4.

Figure 4.10 Test #3: Comparison of measured and predicted force-displacement relationship

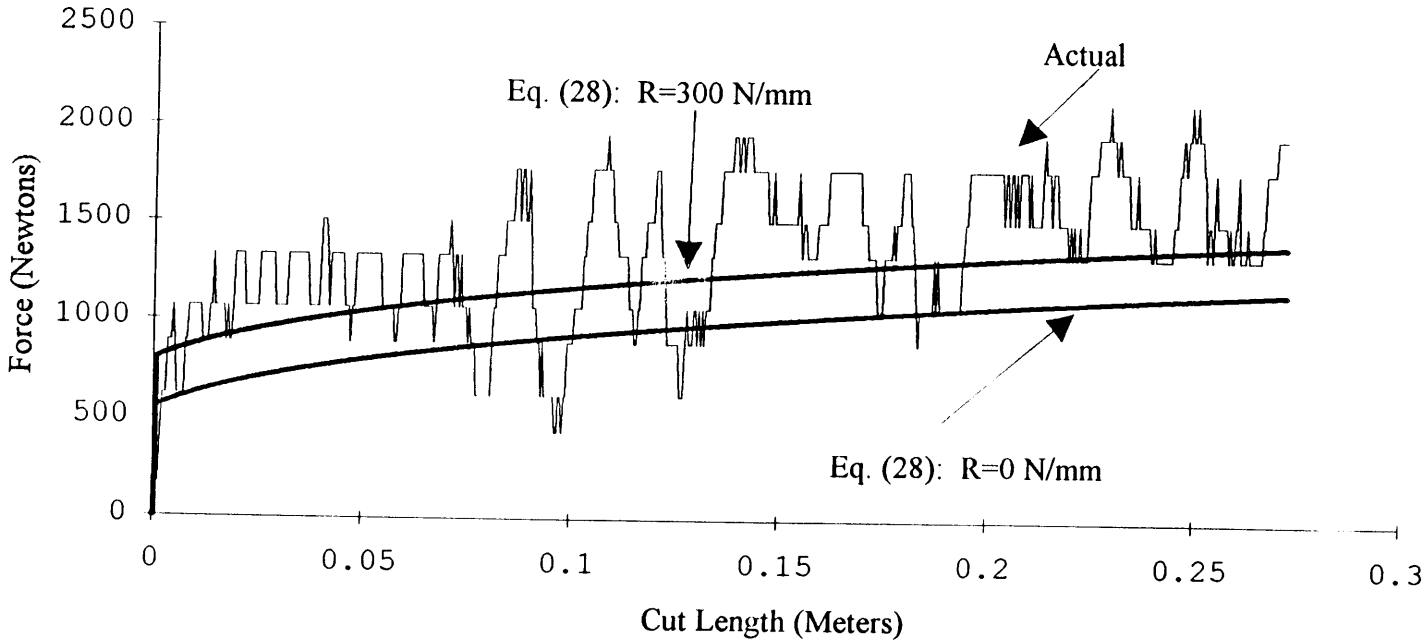

Figure 4.11 Test #4: Comparison of measured and predicted force-displacement relationship

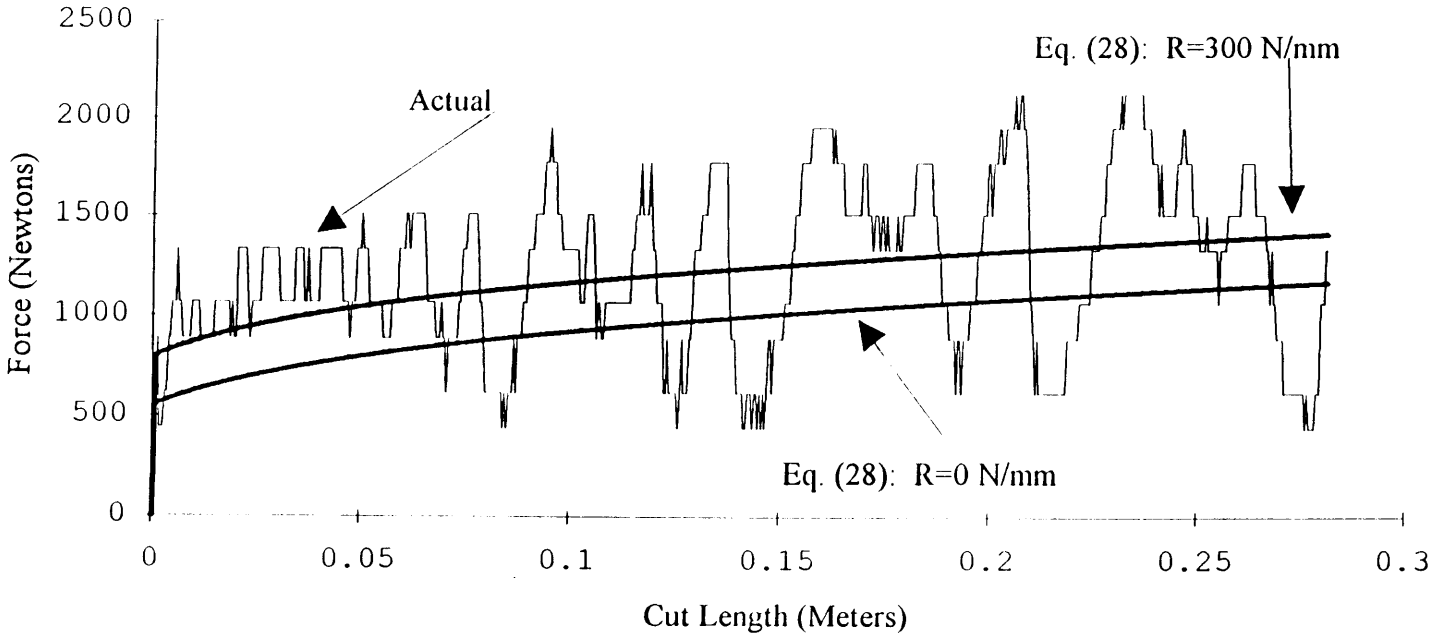

Figure 4.12 Comparison of measured and predicted values of the folding wavelength in tests #3 and #4

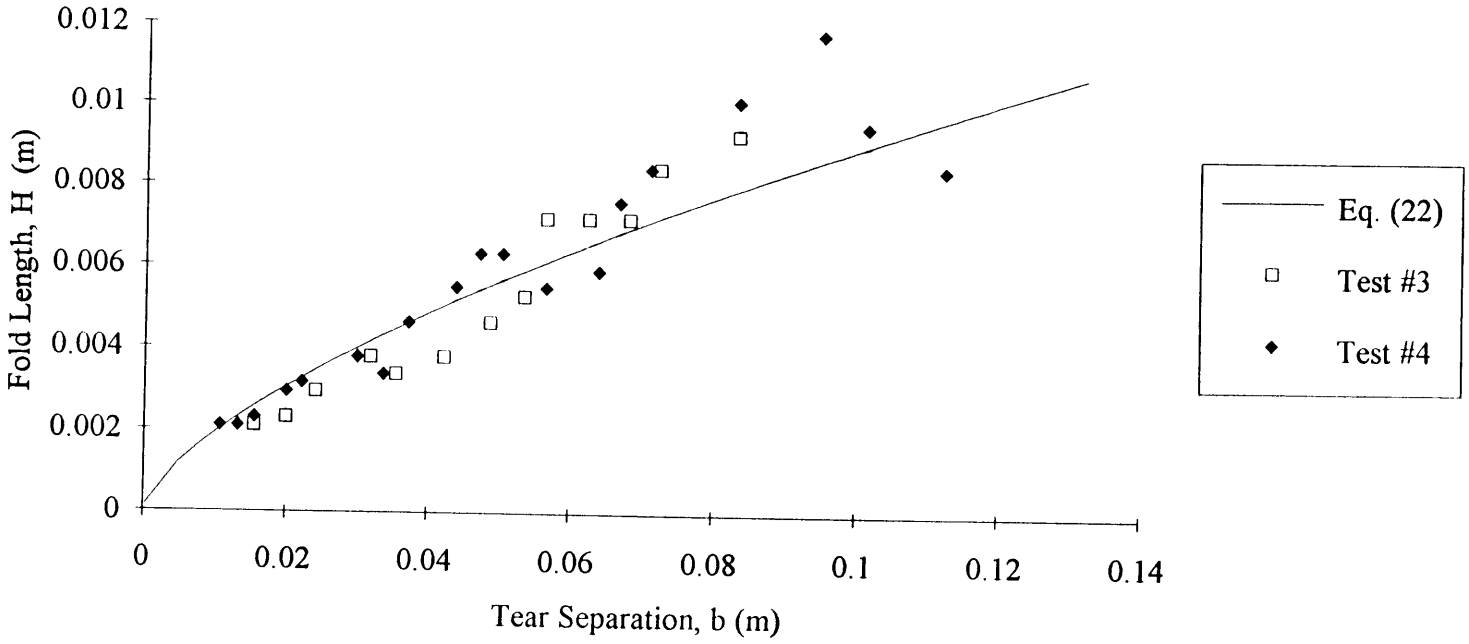

Figure 4.13 Diagram of diverging width with respect to cut length in test #3

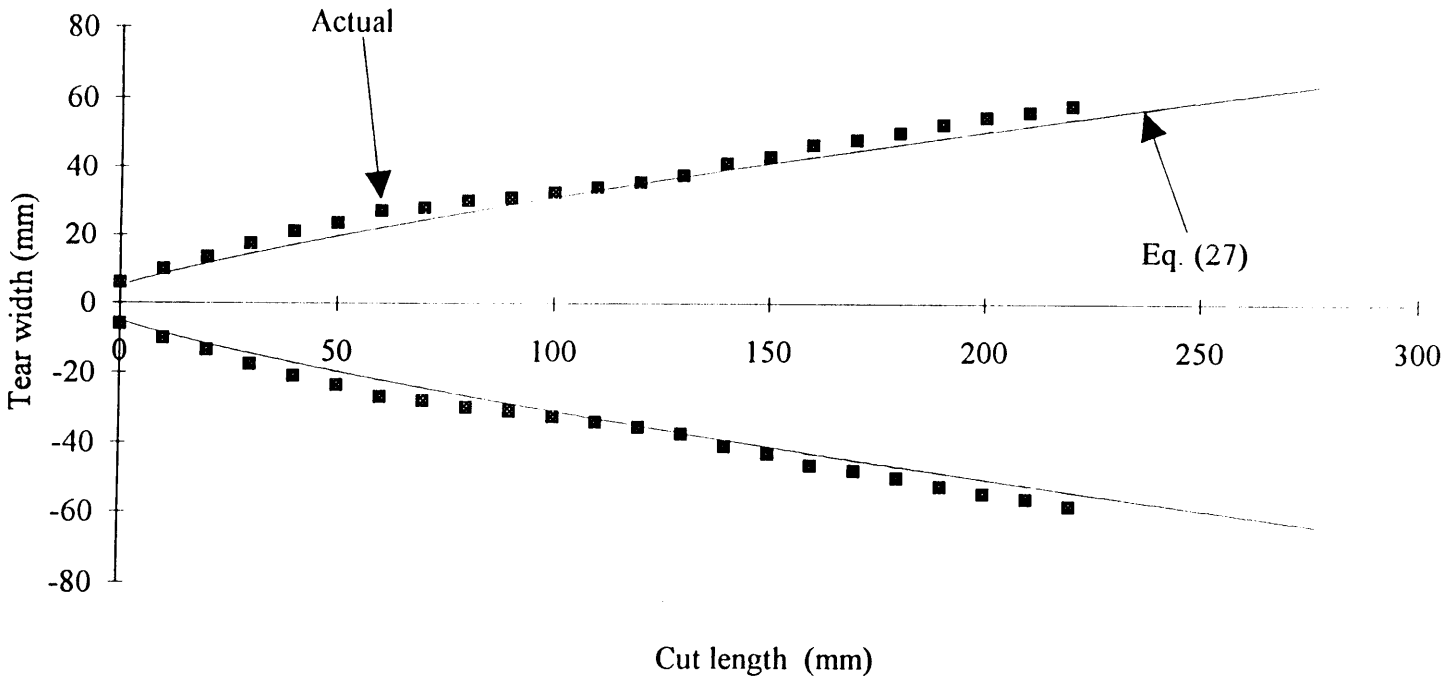

Figure 4.14 Diagram of diverging shape in test #4

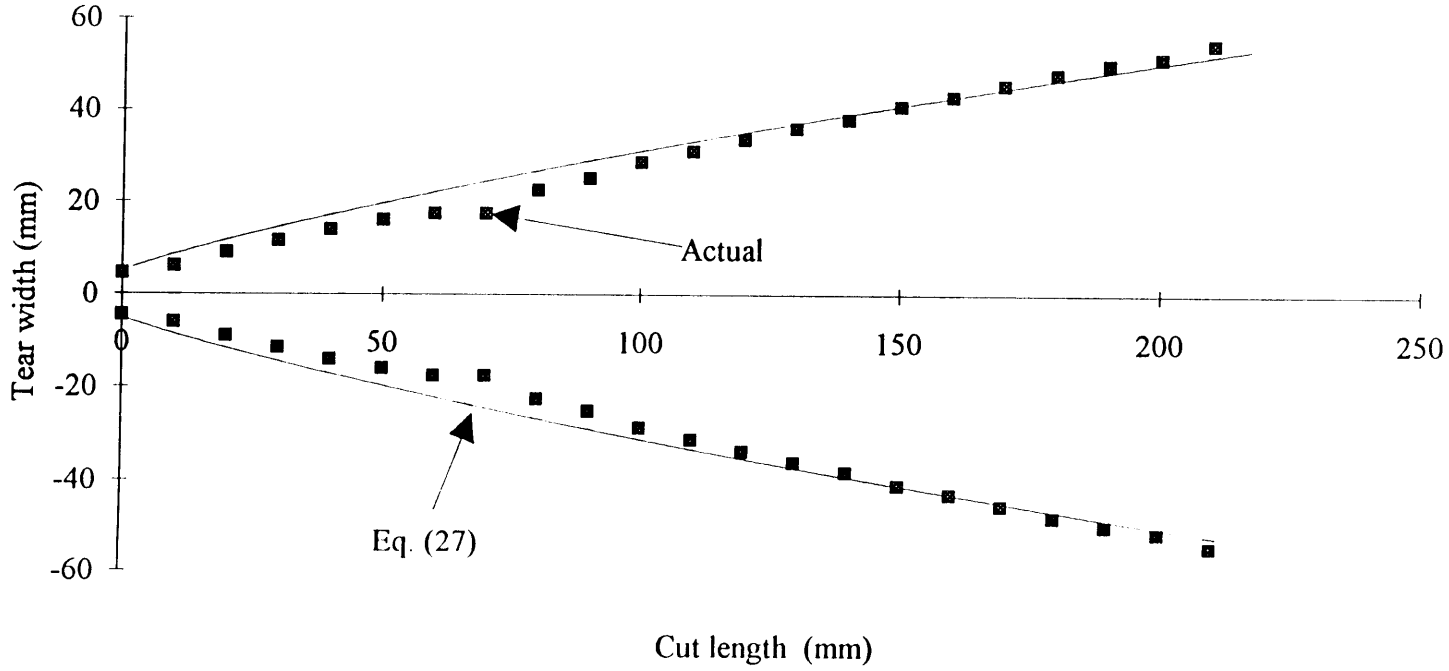

Figure 4.15 A photograph of test #5, diverging concertina with a round wedge.

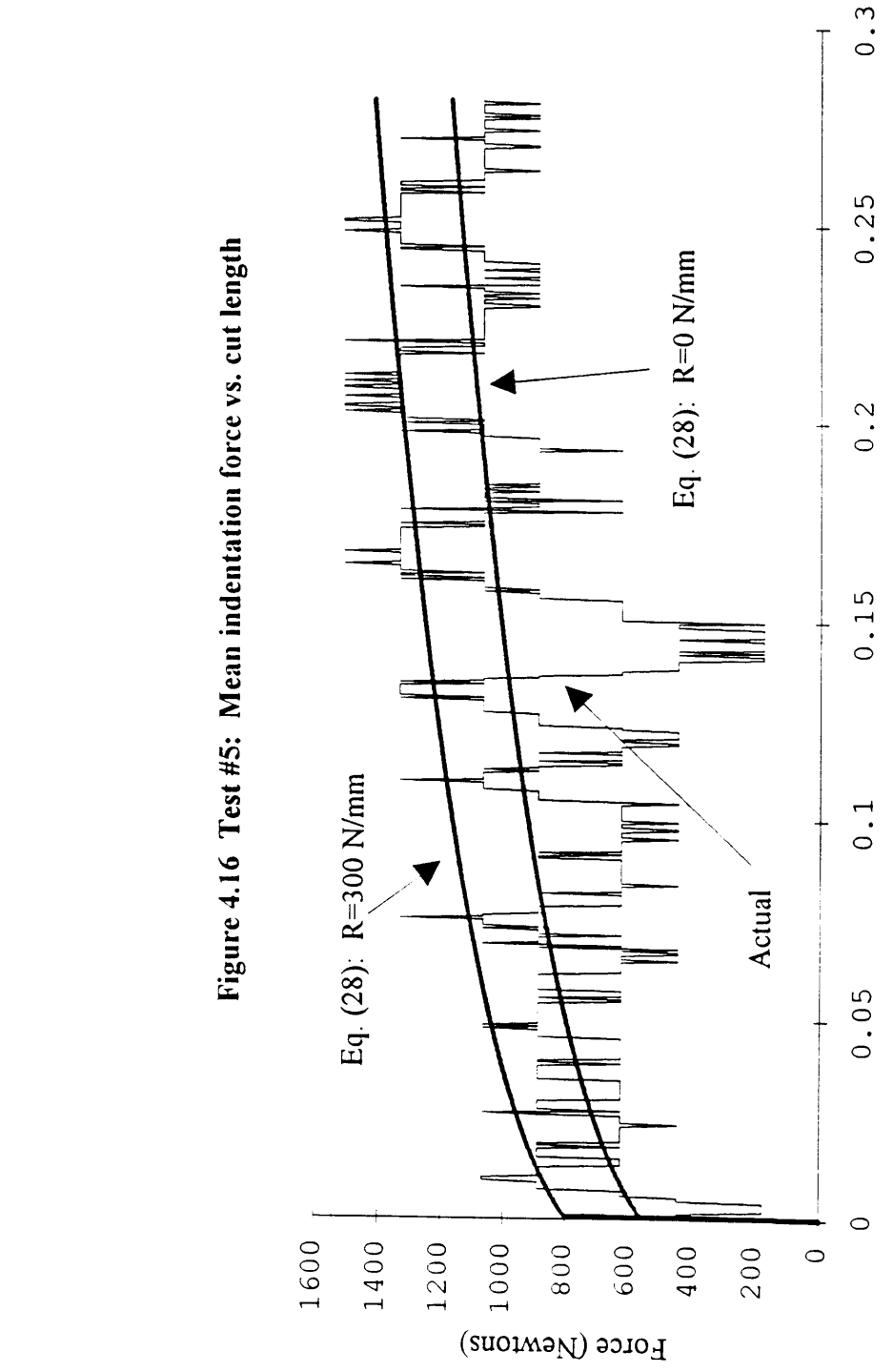

Figure 4.16 Test #5: Mean indentation force vs. cut length

Figure 4.17 Folding wavelength as a function of cut width in test #5

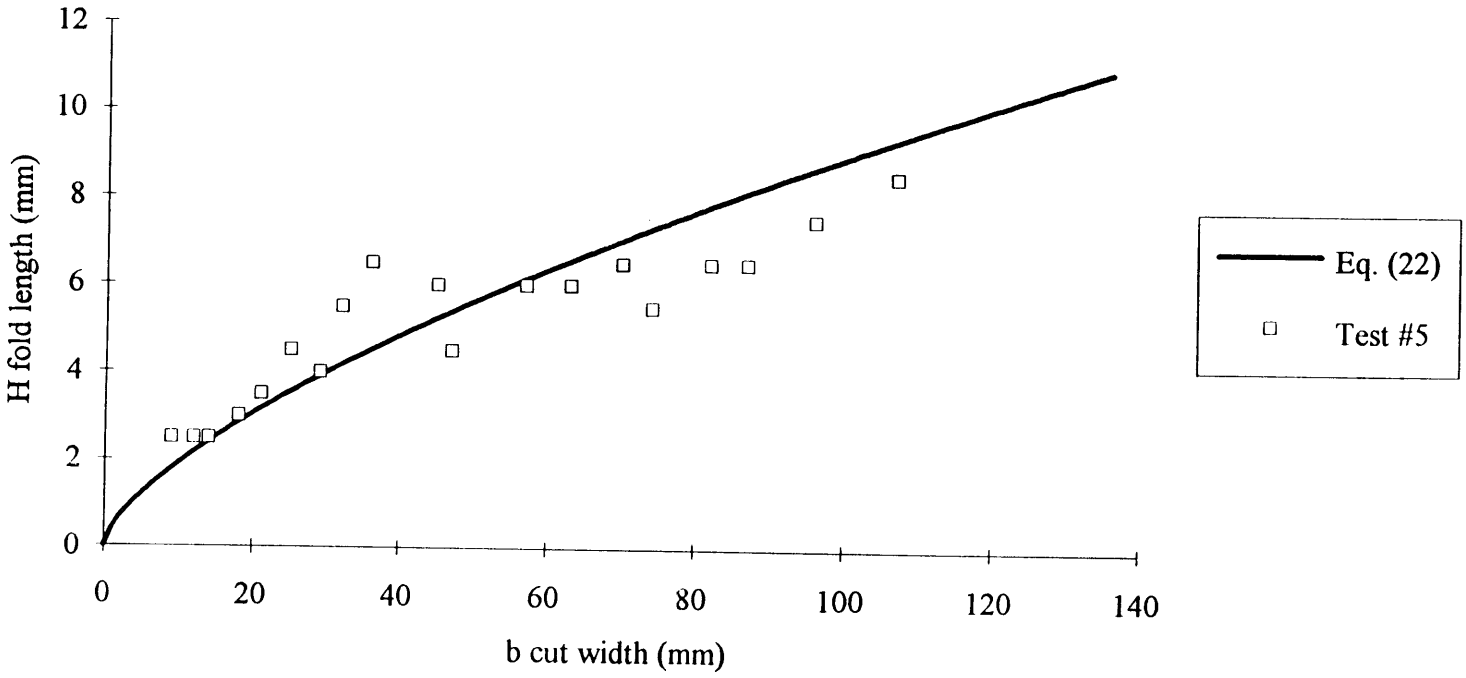

Figure 4.18 The diverging predicted and measured shape for test #5

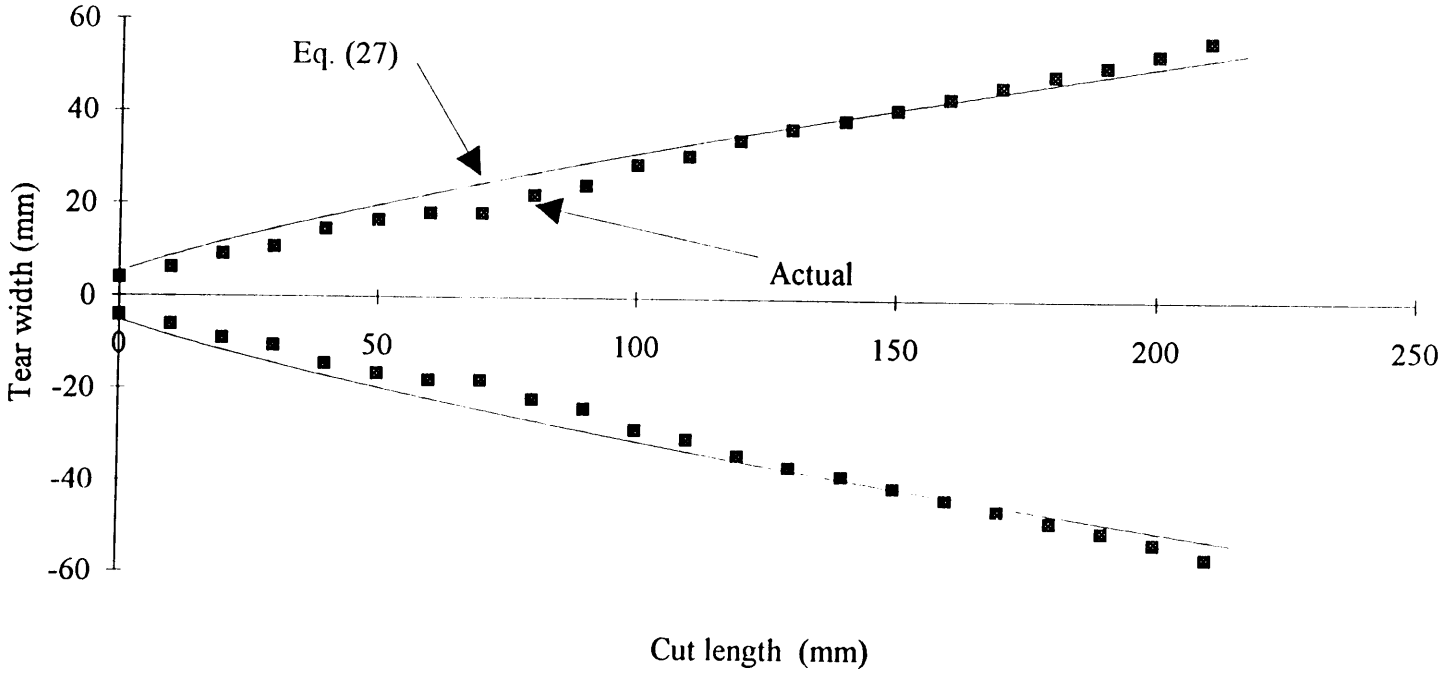

Figure 4.19 A photograph of the deformed specimen #6 at the end of the test.

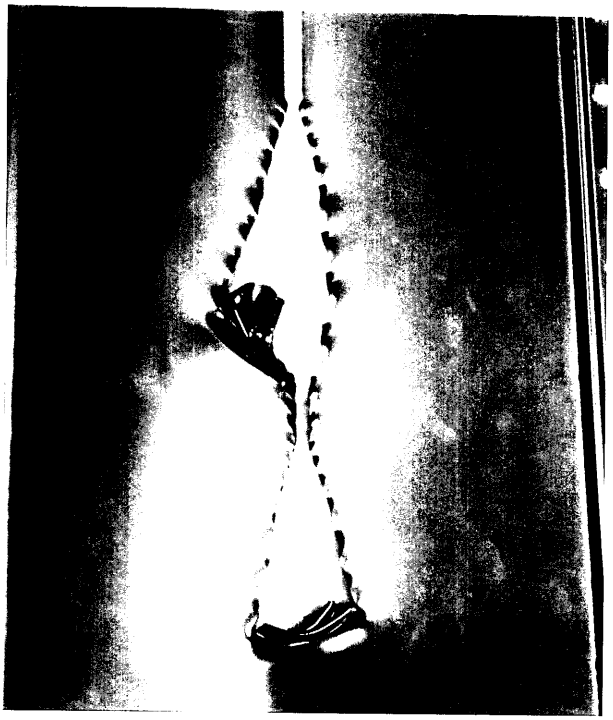

Figure 4.20 A photograph of the deformed specimen #7.

Figure 4.21 Test #6: Comparison of measured and predicted force-displacement relationship

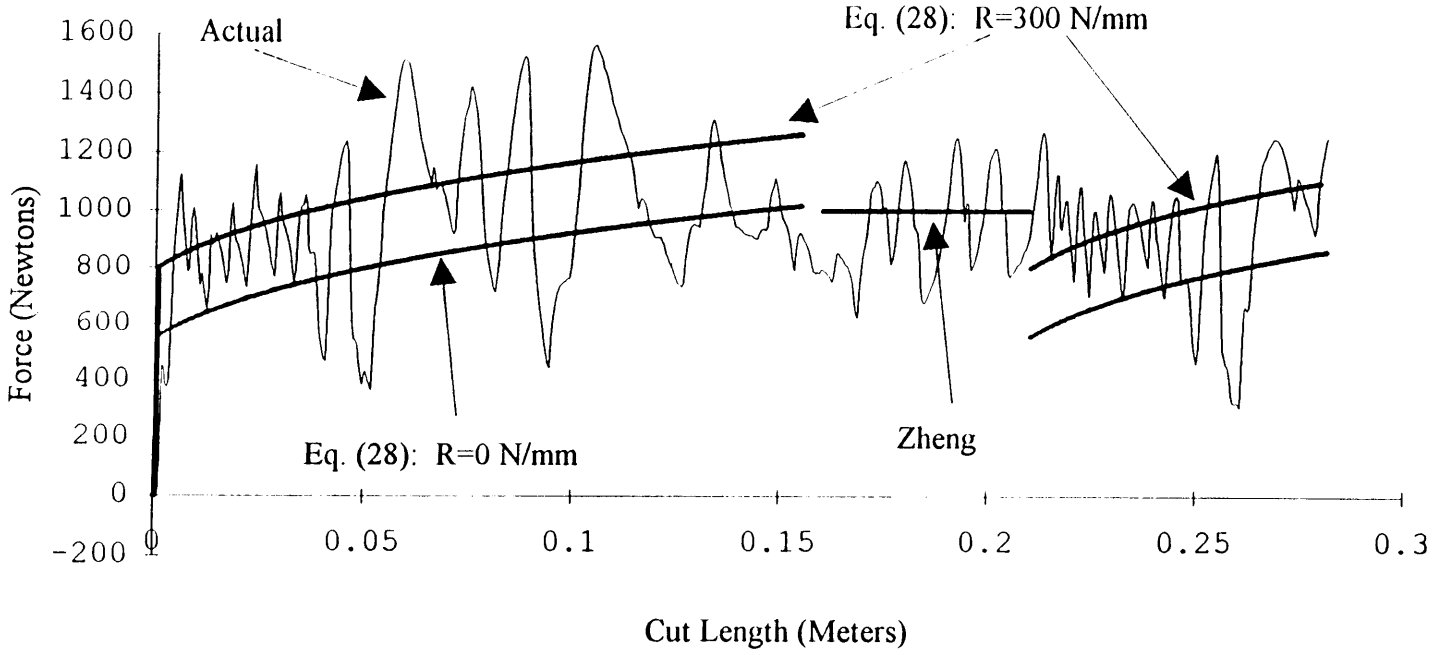

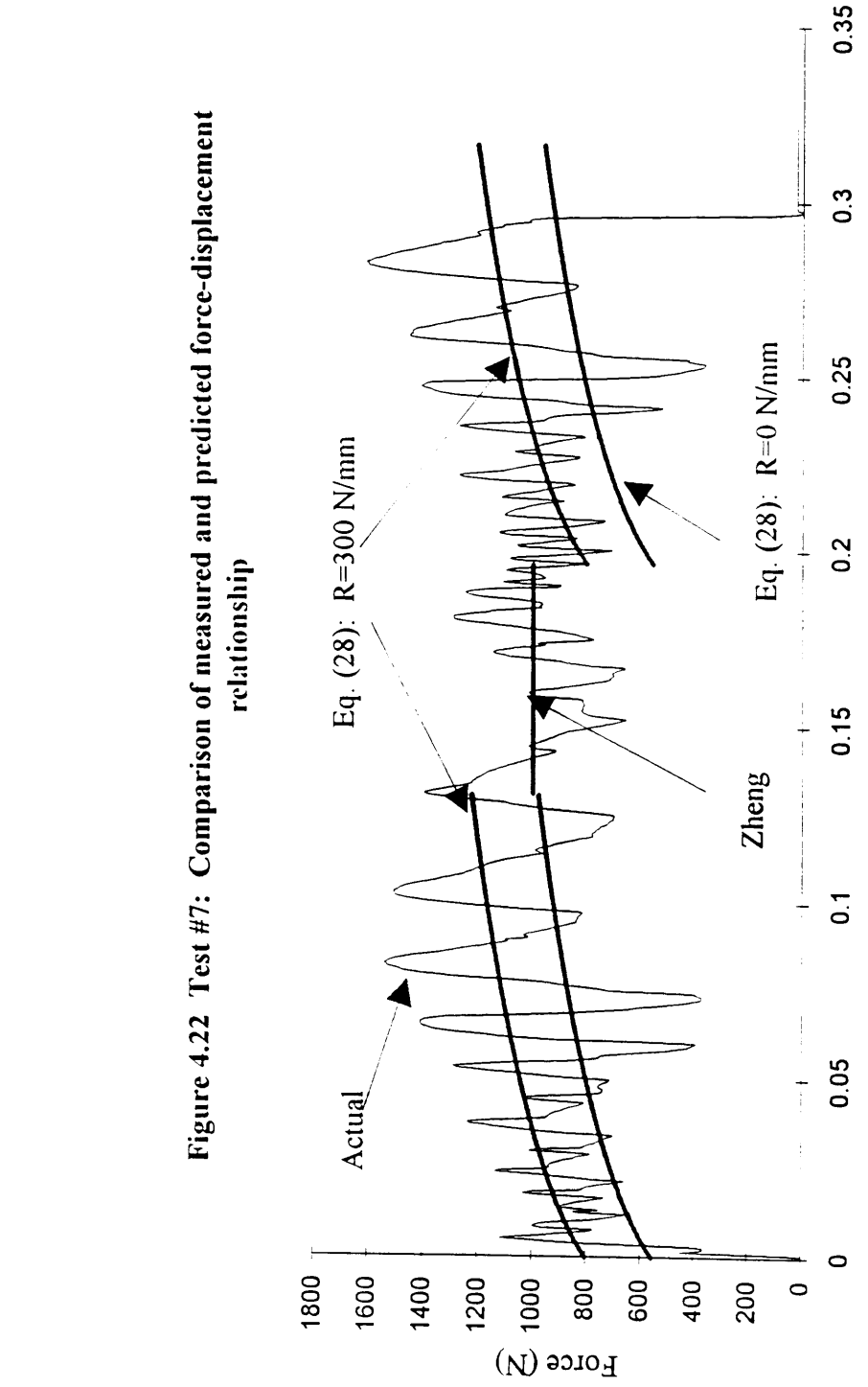

Figure 4.22 Test #7: Comparison of measured and predicted force-displacement relationship

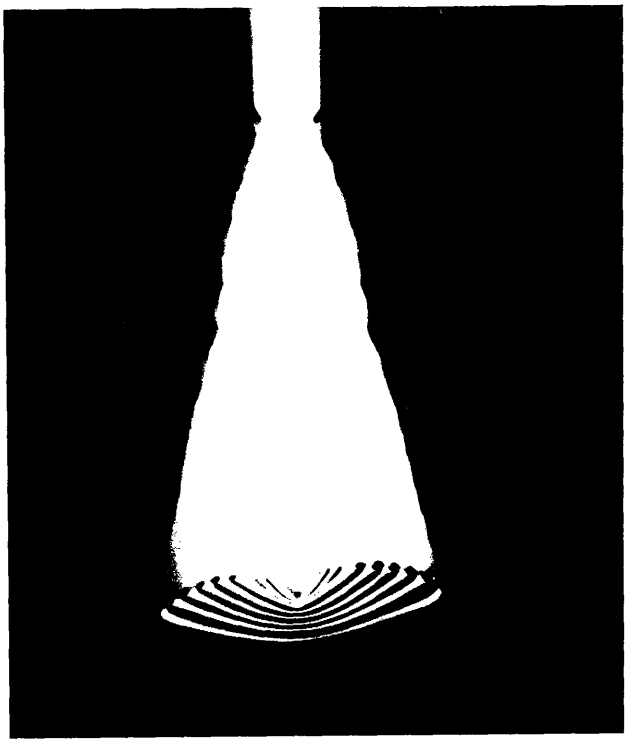

Figure 4.23 A photograph of the deformed specimen #8 at the end of the test.

Figure 4.24 A photograph of the deformed specimen #9.

Figure 4.25 Test #8: Comparison of measured and predicted force-displacement relationship

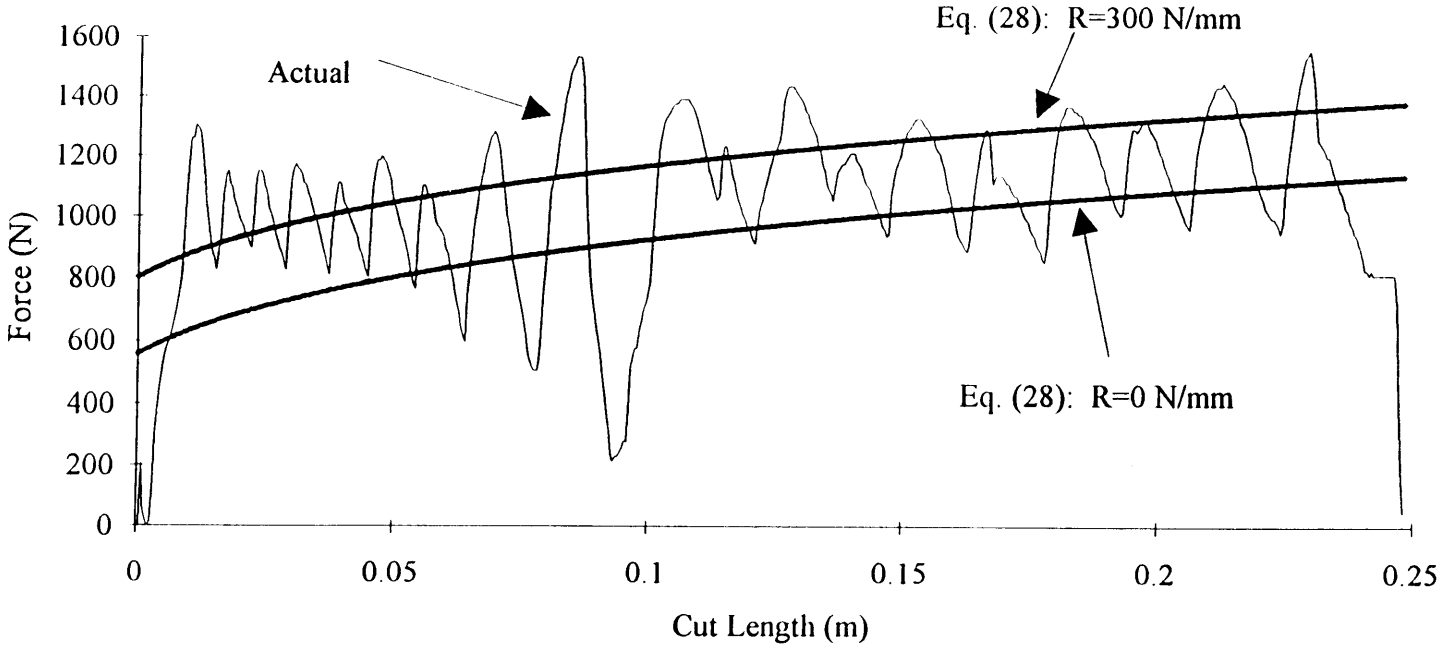

Figure 4.26 Test #9: Comparison of measured and predicted force-displacement relationship

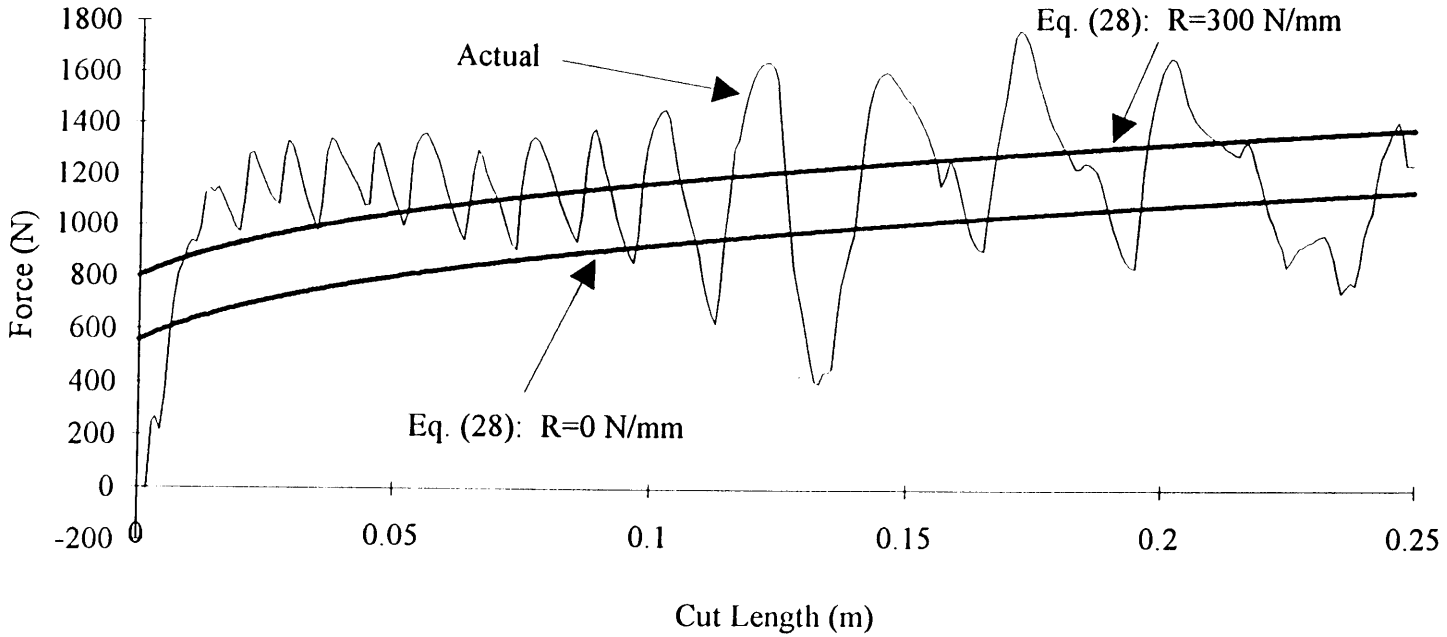

Figure 4.27 Comparison of measured and predicted values of the folding wavelength in tests #8 and #9

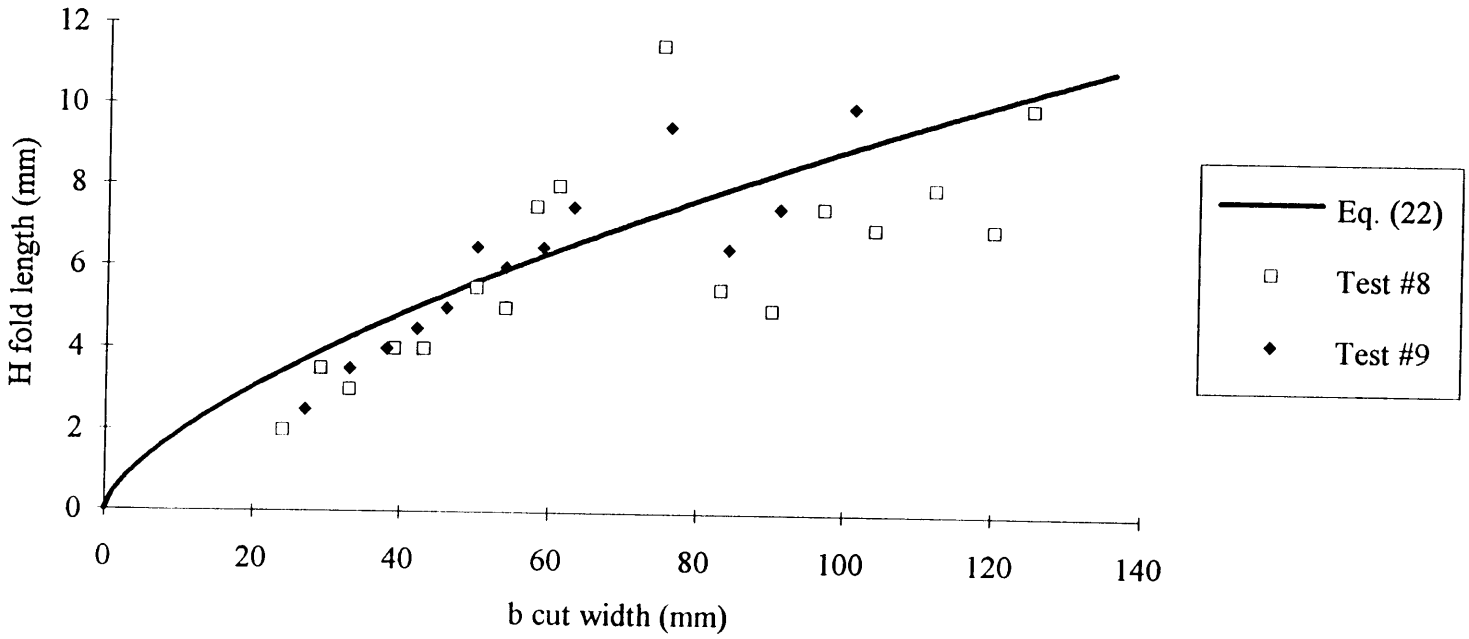

Figure 4.28 Diagram of diverging width with respect to cut length in test #8

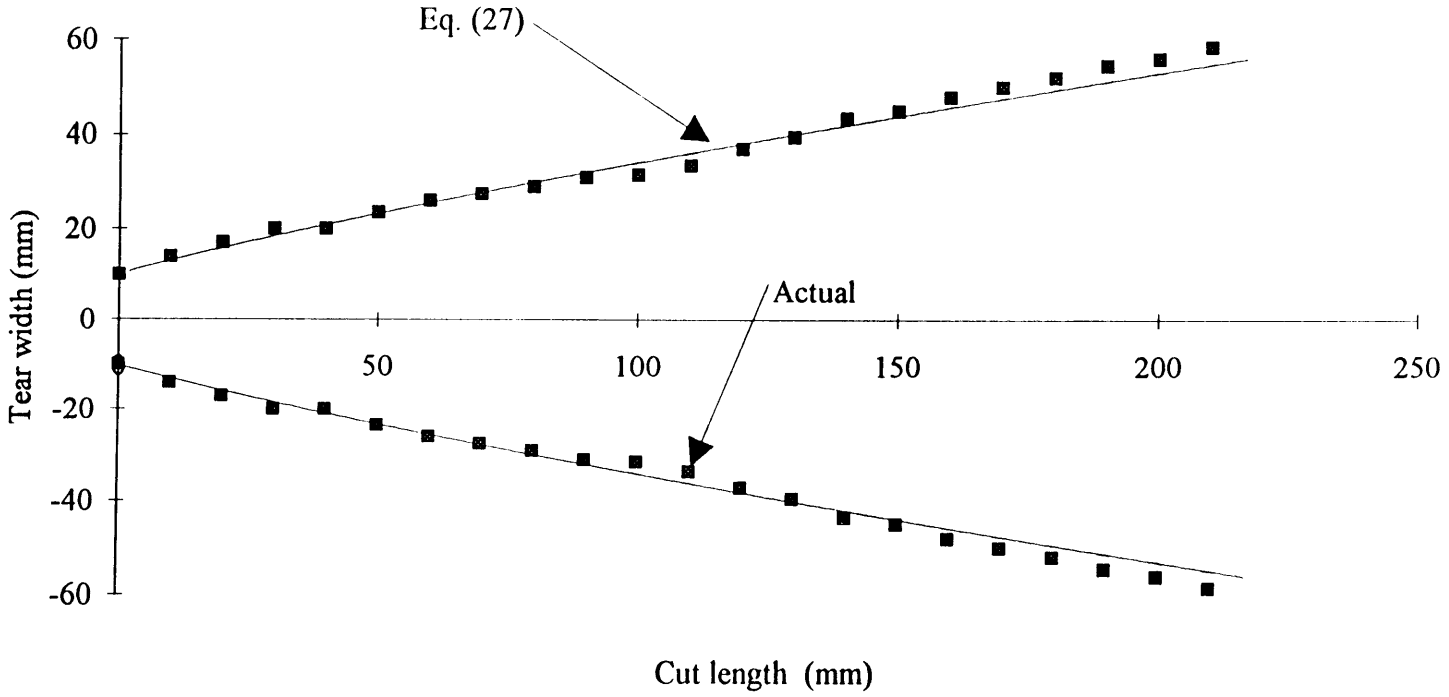

Figure 4.29 Diagram of diverging shape in test #9

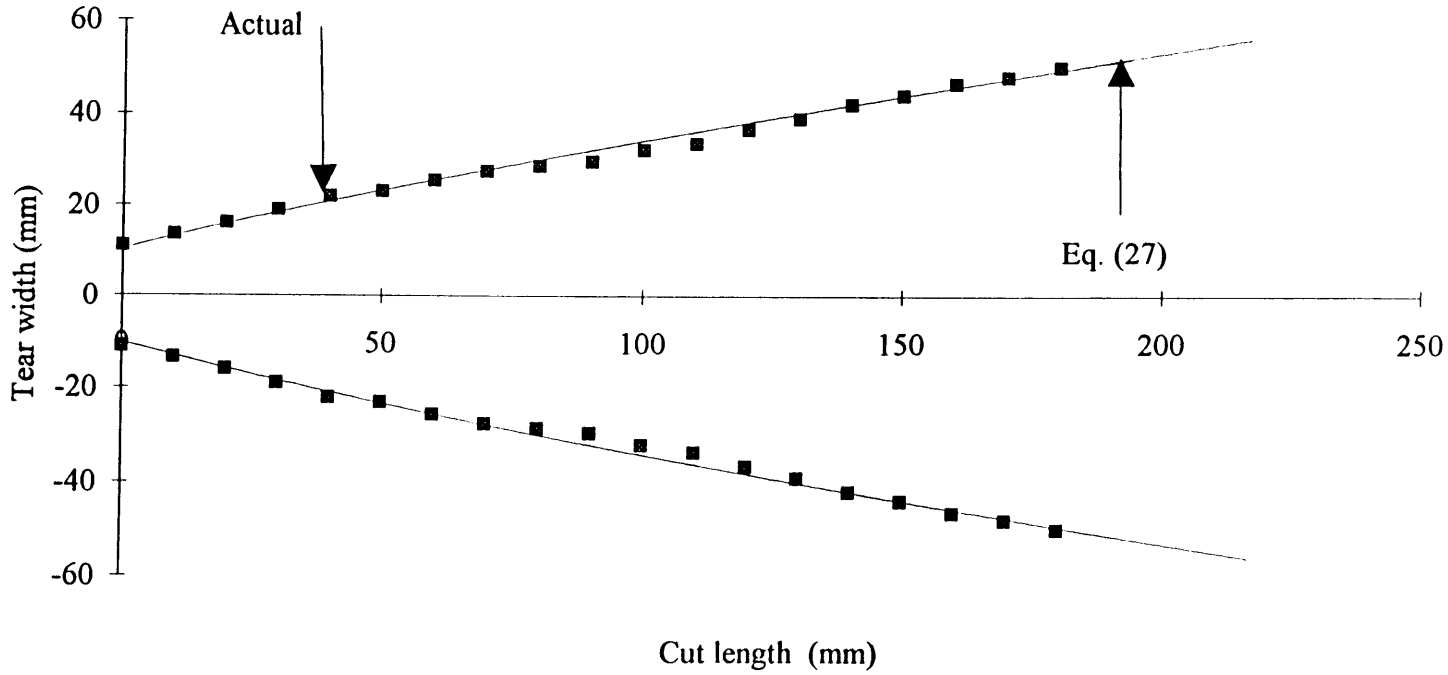

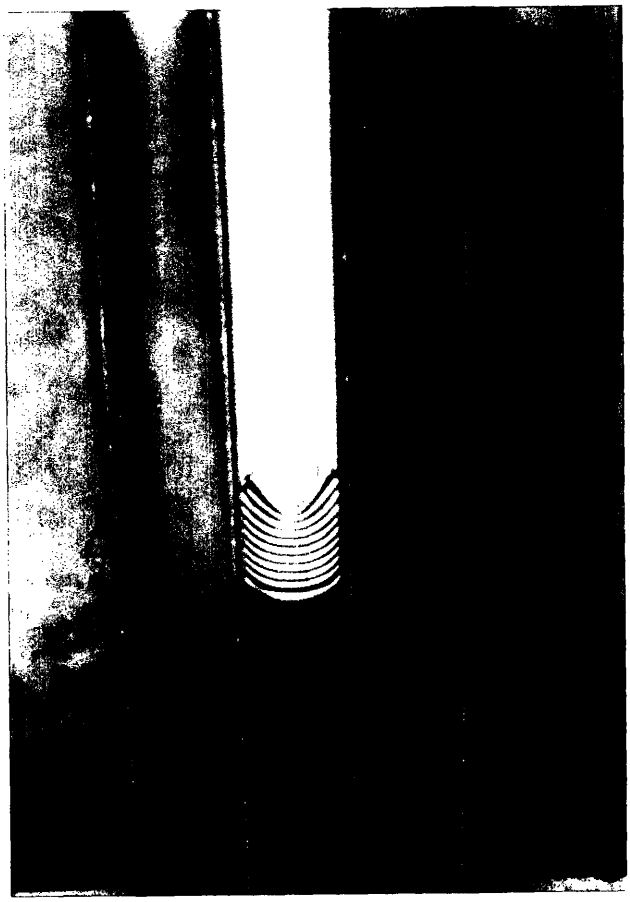

Figure 4.30 A photograph of the bounded concertina tearing, test #10.

Figure 4.31 Test #10: A comparison of mean force vs. displacement

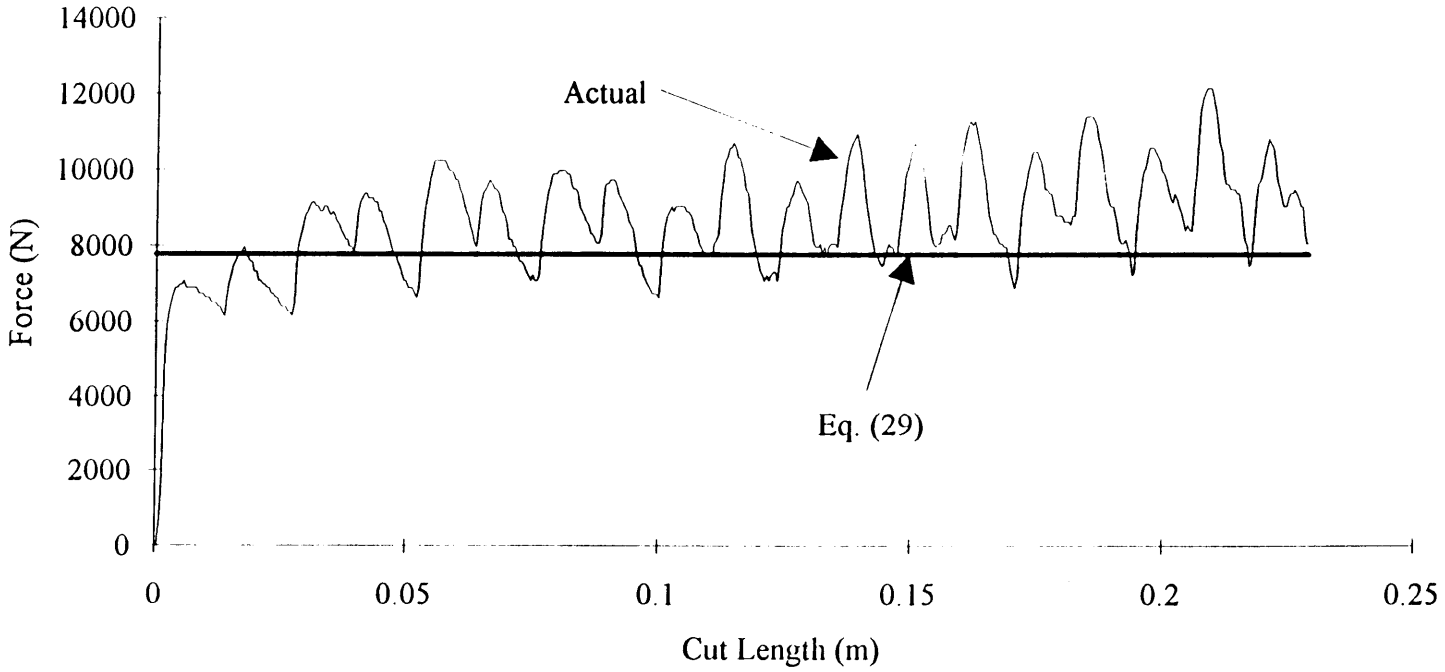

5 Conclusions

In this study, a solution for diverging concertina tearing was derived and 10 tests were conducted to validate this theoretical solution of concertina tearing. The data collected correlated closely with the theory. It was shown that concertina tearing is a valid failure mode for thin sheet steel, and that concertina mode can develop from central tearing. This was unexpected; it was thought that once central tearing was initiated the failure would continue in that mode. It would be expected that the tests with notches cut in the center of the plate would continue in central tearing, but they also went directly into concertina tearing. The results of tests #3 and #4 are of particular interest to the ongoing tanker project, because they simulate a blunt rock piercing the hull more accurately than tests which are initiated at the free edge.

The series of tests #5 through #7 were all conducted using the narrow round wedge, although with widely different results. The first test was nearly identical in all respects to the other diverging tests conducted with the blunt wedge. Tests #6 and #7 showed a multiple failure mode. They alternated between steady state diverging concertina tearing and central cutting, thus demonstrating the similarity between mean force levels for both failure modes.

Tests #8 and #9 demonstrated that diverging concertina tearing is velocity independent, by being nearly identical in both quantitative and qualitative results. The later test was run at twice the velocity of the first, and is virtually indistinguishable from the first.

The final test was a demonstration of bounded concertina (the basis of the diverging theory). This showed that the underlying modeling assumptions describe the

deformation well, and can be expanded upon to derive the diverging shape and mean force equations.

References

1. K. Kitamura, Y.Okumoto and T. Shibue, On the Model Tests of Double Bottom Strength for Standing, (in Japanese) *J. Society of Naval Architects of Japan,* vol. 143, pp. 346-356 (1978).

2. "Congressional Record - House," Vol. 136, No. 102, Part I, U.S. Federal Printing Office, August 1, 1990.

3. "Federal Register," Vol. 55, No. 234, U.S. Federal Printing Office, December 1990.

4. L. Maxwell, Effect of Rock Geometry on the Failure Mode of Plates and The Forces in Grounding Experiments, Joint MIT-Industry Program on Tanker Safety, Report #15, May 1993.

5. G. Nurick, Private Communication. September 1993.

6. T. Wierzbicki, Concertina Tearing of Metal Plates Improved Solution and Comparison with Experiments, Joint MIT-Industry Program on Tanker Safety, Report #22, January 1994.

7. A. G. Atkins, Scaling in Combined Plastic Flow and Fracture. *Int. J. Mech. Sci.* vol. 30, p. 173 (1988).

8. W. J. Stronge, T. X. Yu and W. Johnson, Long Stroke Energy Dissipation in Splitting Tubes, *Int. J. Mech. Sci.* vol. 25, pp. 637-647 (1983).

9. W. Abramowicz, The Effective Crushing Distance in Axially Compressed Thin-walled Metal Columns, *Int. J. Impact Engineering* vol. 1, pp. 309-317 (1983).

10. T. Wierzbicki, Concertina Tearing of Metal Plates, Joint MIT-Industry Program on Tanker Safety, Report #12, March 1993.

11. T. Wierzbicki, and Z. Zheng, Private Communication, January 1994.